

D0 dimuon charge asymmetry from B_s system with Z' couplings and the recent LHCb result

Hyung Do Kim^{1a} Sung-Gi Kim^{2b} and Seodong Shin^{1c}

¹*CTP and Department of Physics and Astronomy,
Seoul National University,
Seoul 151-747, Korea*

²*Physics Department, Indiana University,
Bloomington, IN 47405, USA*

Abstract

The D0 collaboration has announced the observation of the like-sign dimuon charge asymmetry since 2010, which has more than 3σ deviation from the Standard Model prediction. One of the promising explanation is considering the existence of flavor changing Z' couplings to the b and s quarks which can contribute to the off-diagonal decay width in the $B_s - \bar{B}_s$ mixing. Model construction is highly constrained by the recent LHCb data of 1fb^{-1} integrated luminosity. In this paper, we analyze the experimental constraints in constructing new physics models to explain the dimuon charge asymmetry from the CP violation of the B_s system. We present limits on Z' couplings and show that it is impossible to obtain the 1σ range of the dimuon charge asymmetry without the new contribution in the B_d system. Even with arbitrary contribution in the B_d system, the new couplings must be in the fine tuned region.

^a hdkim@phya.snu.ac.kr

^b kimsg@indiana.edu

^c sshin@phya.snu.ac.kr

I. INTRODUCTION

The like-sign dimuon charge asymmetry from the semi-leptonic ($s\ell$) decay of $B_{s,d}$ meson is given by,

$$A_{s\ell}^b = \frac{N^{++} - N^{--}}{N^{++} + N^{--}}, \quad (1)$$

where N^{++} corresponds to each B hadron decaying semi-leptonically to μ^+X , and similarly N^{--} to μ^-X . In 2010, the D0 collaboration at the Tevatron announced the first observation of the large dimuon charge asymmetry, which had about 3.2σ deviation excess from what is expected in the Standard Model (SM) [1]. In 2011, the result from the analysis with 9 fb^{-1} data is announced as [2]

$$A_{s\ell}^b = -(7.87 \pm 1.72 \pm 0.93) \times 10^{-3}, \quad (2)$$

which has about 3.9σ deviation from the SM prediction [2],

$$A_{s\ell}^{b\text{SM}} = (-2.8_{-0.6}^{+0.5}) \times 10^{-4}. \quad (3)$$

To explain the observed asymmetry, we need additional sources of CP violation from the new physics (NP) beyond the SM in the $B_{s,d}$ mixing or decay.

The contribution from each neutral B^0 and B_s^0 meson is parametrized by the flavor specific asymmetry

$$\begin{aligned} a_{s\ell}^d &\equiv \frac{\Gamma(\overline{B}_d \rightarrow \mu^+ X) - \Gamma(B_d \rightarrow \mu^- X)}{\Gamma(\overline{B}_d \rightarrow \mu^+ X) + \Gamma(B_d \rightarrow \mu^- X)}, \\ a_{s\ell}^s &\equiv \frac{\Gamma(\overline{B}_s \rightarrow \mu^+ X) - \Gamma(B_s \rightarrow \mu^- X)}{\Gamma(\overline{B}_s \rightarrow \mu^+ X) + \Gamma(B_s \rightarrow \mu^- X)}. \end{aligned} \quad (4)$$

The fraction of each flavor specific asymmetry in the total asymmetry $A_{s\ell}^b$ at the Tevatron energy 1.96 TeV depends on the mean mixing probabilities and the production fractions of B^0 and B_s^0 mesons such that [2]

$$A_{s\ell}^b = (0.594 \pm 0.022)a_{s\ell}^d + (0.406 \pm 0.022)a_{s\ell}^s, \quad (5)$$

which leads to 6 : 4 production of the like-sign dimuons from the $b\bar{d}(d\bar{b})$ and $b\bar{s}(s\bar{b})$ mesons.¹

¹ This is different from the 2010 prediction of about 5 : 5 production.

Imposing the lower limits of the muon impact parameter (IP), it is possible to reduce the background dramatically, which is mainly from the long-lived charged mother particles of the muon and the anti-muon. In the 2011 data, the separation of the sample by the muon impact parameter induces the separate determination of $a_{s\ell}^d$ and $a_{s\ell}^s$ such that

$$a_{s\ell}^s = -(18.1 \pm 10.6) \times 10^{-3} , \quad (6)$$

$$a_{s\ell}^d = -(1.2 \pm 5.2) \times 10^{-3} , \quad (7)$$

where the SM predictions using the SM fit of $|V_{ub}| = (3.56^{+0.15}_{-0.20}) \times 10^{-3}$ [3] are

$$a_{s\ell}^{s\text{SM}} = (1.9 \pm 0.3) \times 10^{-5} , \quad (8)$$

$$a_{s\ell}^{d\text{SM}} = -(4.1 \pm 0.6) \times 10^{-4} . \quad (9)$$

The separately determined $a_{s\ell}^s$ has about 1.7σ deviation from the SM prediction if $a_{s\ell}^d$ can be freely chosen to fit the data. Similarly the $a_{s\ell}^d$ is within 1σ if $a_{s\ell}^s$ can be arbitrary. It should be emphasized that large contribution from new physics is inevitable if both of $a_{s\ell}^d$ and $a_{s\ell}^s$ are considered.

We reproduced the χ^2 -fit combining the impact parameter cut ($120\mu m$) analysis of $\text{IP}_{<120}$ and $\text{IP}_{>120}$ in Fig. 1. As seen in the figure, we need to consider both of $a_{s\ell}^d$ and $a_{s\ell}^s$ together in the 2D plane. In this figure, we used the central values in the fraction of contribution by $a_{s\ell}^d$ and $a_{s\ell}^s$ in $A_{s\ell}^b$, shown in [2]. In Fig. 1 (b), the required NP contribution is expressed in terms of $a_{s\ell}^d/(a_{s\ell}^d)^{\text{SM}}$ (number at the horizontal arrow) or $-a_{s\ell}^s/(a_{s\ell}^s)^{\text{SM}}$ (numbers at the vertical arrows). The red dot denotes the observed central value of $(a_{s\ell}^d, a_{s\ell}^s)$. Without NP contribution to $a_{s\ell}^d$, the enhancement $-a_{s\ell}^s/(a_{s\ell}^s)^{\text{SM}} > 580$ is needed to explain the asymmetry within 1σ . Even if we allow arbitrarily large new physics in $a_{s\ell}^d$, we still need at least 68 times bigger size of $a_{s\ell}^s$ to explain the asymmetry within 1σ where $a_{s\ell}^d/(a_{s\ell}^d)^{\text{SM}} = 21$ at the 1σ boundary. To be in the central point in which the χ^2 fit is the best, $a_{s\ell}^s$ should be enhanced by a factor of 950 while small enhancement in $a_{s\ell}^d/(a_{s\ell}^d)^{\text{SM}} < 3$ is enough. Therefore, we cannot explain the dimuon charge asymmetry within 1σ in the χ^2 -fit without large NP contribution in $a_{s\ell}^s$.²

To investigate the possibility accommodating such large new CP violating contribution in the $B_s - \bar{B}_s$ mixing system for the dimuon charge asymmetry within 1σ in the χ^2 -fit, we

² If we aim for the asymmetry within 90% confidence region (1.65σ) or 2σ region, the observation result can be achieved only by the enhancement in $a_{s\ell}^d$ without having any contribution in $a_{s\ell}^s$.

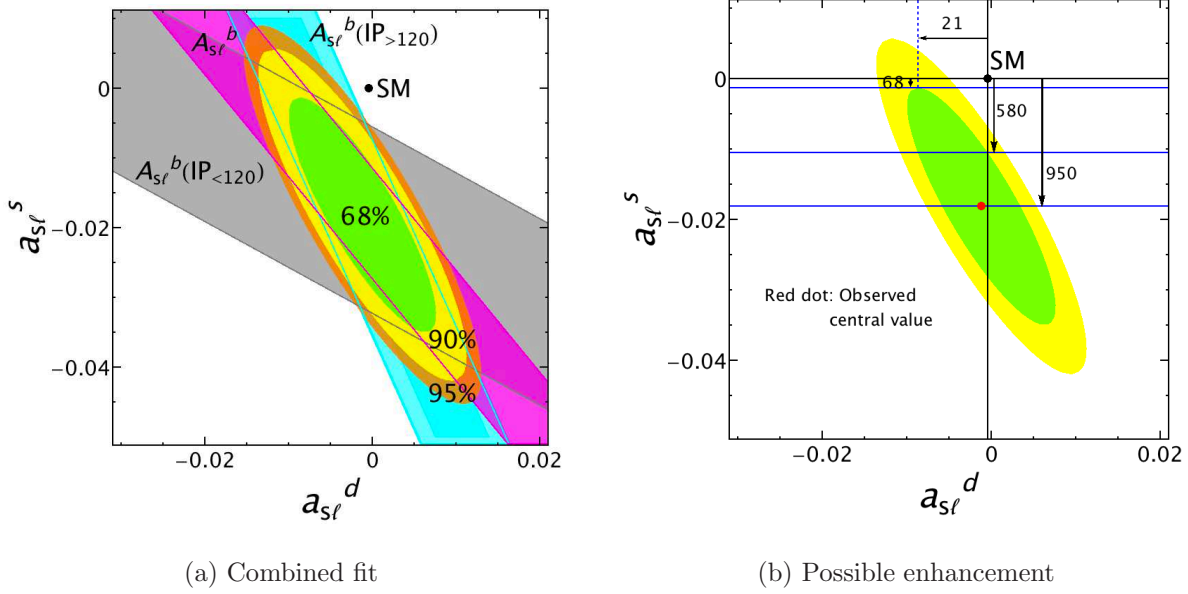


FIG. 1. We reproduced the measurements with different muon impact parameter (IP) selections according to [2] in (a). The bands are the 90% uncertainties on each individual measurement of $\text{IP}_{<120}$ (Gray), $\text{IP}_{>120}$ (Cyan), and the result without the IP cut (Purple) in (2). The green (68%), yellow (90%), and orange (95%) ellipses are obtained from the χ^2 -fit combining the measurements of $\text{IP}_{<120}$ and $\text{IP}_{>120}$ using the independent data sample. To explain the asymmetry within 1σ in the $(a_{s\ell}^d, a_{s\ell}^s)$ plane, the required NP contribution is expressed in terms of $a_{s\ell}^d/(a_{s\ell}^d)^{\text{SM}}$ (number at the horizontal arrow) or $-a_{s\ell}^s/(a_{s\ell}^s)^{\text{SM}}$ (numbers at the vertical arrows) in (b). The red dot denotes the observed central value of $(a_{s\ell}^d, a_{s\ell}^s)$.

will take three points explained in Fig. 1 (b) as reference ones.

$$(a_{s\ell}^d/(a_{s\ell}^d)^{\text{SM}}, a_{s\ell}^s/(a_{s\ell}^s)^{\text{SM}}) = (21, -68), (1, -580), (1, -950), \quad (10)$$

where the small enhancement in $a_{s\ell}^d$ at the third reference point is not considered.

Such asymmetry has been explained in the context of many new physics models. One of the simplest approaches is considering the flavor violating interaction of b and s quarks with an additional U(1) neutral gauge boson Z' , which enhances the off-diagonal decay width Γ_{12} from the absorptive part of the $B_s - \bar{B}_s$ mixing [4, 5]. A set-up considering the new $(\bar{s}b)(\bar{\tau}\tau)$ operator is promising to enhance the Γ_{12} since the NP contributions to $b \rightarrow s\tau^+\tau^-$ processes have relatively weak experimental constraints from the $\text{Br}(B_s \rightarrow \tau^+\tau^-)$ [6]. The other approach is considering the interference of the Z' to c -quark pair interaction and the SM process exchanging the charged W boson [5]. In general models with new Γ_{12} , the

enhancement of the asymmetry can be achieved by the $\text{Im}(\Gamma_{12})$ without suffering from the experimental constraint of width difference $\Delta\Gamma$ depending on the $\text{Re}(\Gamma_{12})$, which will be discussed in Sec. III B.

On the other hand, the existence of the extra gauge boson Z' induces the tree level flavor changing neutral current (FCNC) from the nonzero off-diagonal Z' gauge couplings. Therefore, the Z' model constructions usually suffer from various experimental constraints including B/B_s meson decays³. Especially, the recent LHCb results provided very strong bounds. This situation applies to other NP cases as well.

In this paper, we analyze the effect of such experimental results in constructing the NP explaining the dimuon charge asymmetry. As a promising example, we investigate the Z' models to obtain the bounds in terms of the NP couplings⁴.

This paper is organized as follows. We provide a summary review of the Z' explanation on the dimuon charge asymmetry in Sec. II. Then, we analyze the current experimental bounds constraining the NP model construction explaining the asymmetry and apply the bounds to the Z' properties in Sec. III. The experimental results we will analyze contain the measurements of the mass difference ΔM_s and the width difference $\Delta\Gamma_s$ after the mixing. We also included the bounds from the CP violating phase $\phi_s^{J/\psi\phi}$ of the $B_s \rightarrow J/\psi\phi$ process, the inclusive $b \rightarrow s\nu\bar{\nu}$, and the $\sin 2\beta$ from the golden plate $B \rightarrow J/\psi K_S$. In Sec. IV and V, we directly obtain the combined constraint on the Z' model parameters in the models with the $Z'\tau^+\tau^-$ coupling and the $Z'\bar{c}c$ coupling, respectively. Finally, we give the conclusions in Sec. VI.

II. THE LIKE-SIGN DIMUON CHARGE ASYMMETRY

The $B_q - \bar{B}_q$ oscillations for $q = s, d$ are described by a Schrödinger equation

$$i\frac{d}{dt}\begin{pmatrix} |B^0\rangle \\ |\bar{B}^0\rangle \end{pmatrix} = \left(M - i\frac{\Gamma}{2}\right)\begin{pmatrix} |B^0\rangle \\ |\bar{B}^0\rangle \end{pmatrix}, \quad (11)$$

where M and Γ are the 2×2 Hermitian mass and decay matrices, which are dispersive and absorptive parts in the time dependent mixing respectively. The differences of masses and

³ If there is mixing with the Z boson, the electroweak precision result demands the existence of rather heavy Z' from E₆ [7]. We do not consider such mixing in this paper.

⁴ While we were in the completion of our work, similar analysis in special cases has been done [8].

widths of the physical eigenstates are given by the off-diagonal elements as [9]

$$\Delta M_q = 2|M_{12}^q|, \quad \Delta \Gamma_q = 2|\Gamma_{12}^q| \cos \phi_q, \quad (12)$$

up to numerically irrelevant corrections of order m_b^2/M_W^2 as long as $\Delta M \gg \Delta \Gamma$ for B_q meson system. The CP phase difference between these quantities is defined as

$$\phi_q = \text{Arg.} \left(-\frac{M_{12}^q}{\Gamma_{12}^q} \right), \quad (13)$$

where the SM contribution to this angle is [3]

$$\phi_d^{\text{SM}} = (-7.5 \pm 2.4) \times 10^{-2}, \quad \phi_s^{\text{SM}} = (3.8 \pm 1.1) \times 10^{-3}. \quad (14)$$

The flavor specific charge asymmetry $a_{s\ell}^q$ is related to the mass and width differences in the $B_q - \bar{B}_q$ system as

$$a_{s\ell}^q = \text{Im} \frac{\Gamma_{12}^q}{M_{12}^q} = \frac{|\Gamma_{12}^q|}{|M_{12}^q|} \sin \phi_q = \frac{\Delta \Gamma_q}{\Delta M_q} \tan \phi_q. \quad (15)$$

For the case of $a_{s\ell}^s$, the experimental value of ΔM_s obtained from the LHCb 0.34fb^{-1} with 68.3% C.L. is

$$\Delta M_s = 17.725 \pm 0.041(\text{stat.}) \pm 0.026(\text{sys.}) \text{ ps}^{-1}. \quad (16)$$

The combined result of CDF and D0 is $\Delta M_s = 17.78 \pm 0.12 \text{ ps}^{-1}$, while the SM value is $(\Delta M_s)^{\text{SM}} = (17.3 \pm 2.6) \text{ ps}^{-1}$ [3, 10]. Therefore, the observed value of ΔM_s has not so much deviated from the SM prediction. Without considering the NP contribution to Γ_{12}^s , it is impossible to obtain the observed central value of $a_{s\ell}^s$ from Eqs. (15) and (16) for $q = s$ even we assume $\sin \phi_s = -1$. With the recent LHCb bound from $B_s \rightarrow J/\psi \phi$, the maximally possible enhancement of $a_{s\ell}^s$ in this case is outside the boundary of 1σ of the observed value in (10) as seen in Fig. 3 (b). Therefore, an additional NP contribution to Γ_{12}^s is preferred to explain the like-sign dimuon charge asymmetry through the $B_s - \bar{B}_s$ mixing.

To probe the NP contribution, we split Γ_{12} or M_{12} to the SM and NP contributions as

$$\frac{\Gamma_{12}^{\text{NP}}}{\Gamma_{12}^{\text{SM}}} \equiv \tilde{h}_q e^{i2\tilde{\sigma}_q}, \quad \frac{M_{12}^{\text{NP}}}{M_{12}^{\text{SM}}} \equiv h_q e^{i2\sigma_q}, \quad (17)$$

for real and non-negative parameters \tilde{h}_q and h_q , with the phases constrained in the region, $0 \leq \sigma_q, \tilde{\sigma}_q \leq \pi$. Then, the flavor specific charge asymmetry is given by [4]

$$a_{s\ell}^q = \frac{|\Gamma_{12}^{q\text{SM}}|}{|M_{12}^{q\text{SM}}|} \frac{1}{1 + h_q^2 + 2h_q \cos 2\sigma_q} \times \left[\left\{ -\tilde{h}_q \sin 2\tilde{\sigma}_q (1 + h_q \cos 2\sigma_q) + h_q \sin 2\sigma_q (1 + \tilde{h}_q \cos 2\tilde{\sigma}_q) \right\} \cos \phi_q^{\text{SM}} + \left\{ (1 + \tilde{h}_q \cos 2\tilde{\sigma}_q)(1 + h_q \cos 2\sigma_q) + h_q \tilde{h}_q \sin 2\sigma_q \sin 2\tilde{\sigma}_q \right\} \sin \phi_q^{\text{SM}} \right]. \quad (18)$$

Therefore, the ratio is given by

$$-a_{s\ell}^q / (a_{s\ell}^q)^{\text{SM}} = \frac{1}{1 + h_q^2 + 2h_q \cos 2\sigma_q} \times \left[\left\{ \tilde{h}_q \sin 2\tilde{\sigma}_q (1 + h_q \cos 2\sigma_q) - h_q \sin 2\sigma_q (1 + \tilde{h}_q \cos 2\tilde{\sigma}_q) \right\} \cot \phi_q^{\text{SM}} - \left\{ (1 + \tilde{h}_q \cos 2\tilde{\sigma}_q)(1 + h_q \cos 2\sigma_q) + h_q \tilde{h}_q \sin 2\sigma_q \sin 2\tilde{\sigma}_q \right\} \right]. \quad (19)$$

The factor $1/(1 + h_q^2 + 2h_q \cos 2\sigma_q)$ is fixed by the ratio of $\Delta M_q^{\text{SM}}/\Delta M_q$, near to 1. Therefore, we see that the sizable contribution to $|\Gamma_{12}^{q\text{NP}}/\Gamma_{12}^{q\text{SM}}| = \tilde{h}_q$ can take the dominant role in explaining the observed dimuon charge asymmetry.

The Z' models to enhance the $a_{s\ell}^s$ require the existence of nonzero off-diagonal couplings g_{sb}^L and g_{sb}^R , where $g_{\psi\chi}^{L,R}$ is the coupling of Z' to fermions $\psi_{L,R}$ and $\chi_{L,R}$. Turning off one of the couplings g_{sb}^L and g_{sb}^R for simplicity, this scenario demands the existence of rather large couplings $|g_{\tau\tau}^{L,R}| > 1$ to explain the asymmetry within 1σ range from the observed central value due to the strict ΔM_s constraint. The situation is the same even in the case that the mass of Z' is similar to that of the Z boson. Such large $g_{\tau\tau}^{L,R}$ couplings can violate the observations in the electroweak precision test (EWPT). Therefore, we need to turn on both of the flavor changing couplings g_{sb}^L and g_{sb}^R . The scenario considering the $g_{\tau\tau}^{L,R}$ couplings to explain the dimuon charge asymmetry will be called as “ $g_{\tau\tau}$ scenario” in this paper.

On the other hand, considering the nonzero Z' coupling to the charm quark pair can also explain the dimuon charge asymmetry by considering the interference of the NP contribution and the SM process. Due to the interference, the couplings $g_{sb}^{L,R} g_{cc}^{L,R}$ contribute to $a_{s\ell}^s$ linearly while $g_{s,b}^{L,R} g_{\tau\tau}^{L,R}$ do quadratically so that the interference effect dominates the enhancement of $a_{s\ell}^s$ unless the NP contribution is larger than that of the SM. Therefore, it is possible to explain the asymmetry with rather smaller Z' couplings in this scenario so that we can

avoid the direct constraint such as the decay of $B_s \rightarrow DD_s$ [5]. The scenario considering such contribution will be called as “ g_{cc} scenario” in this paper.

Every experimental result is independent of the mass of Z' unless it makes the couplings too large ⁵. This is because every new interaction depends on the ratio $\rho_{\psi\chi}^{L,R} \equiv \left| (g_{\psi\chi}^{L,R}/g_1)(M_Z/M_{Z'}) \right|$, where $g_1 = g/\cos\theta_W$ for g is the $SU(2)_L$ coupling, and θ_W is the weak mixing angle. However, we sometimes need the exact bounds in the values of the couplings themselves to understand the situation easily. Therefore, we set $M_{Z'} \approx M_Z$ in this paper for the representation of our analyses so that one can simply compare our result with other considerations of $M_{Z'}$. Our simple assumption of $M_{Z'}$ is not unrealistic since the b -quark forward-backward asymmetry A_{FB}^b at the LEP can be explained in terms of Z' where $M_{Z'} \approx M_Z$ and the non-zero $g_{ee}^{L,R}$ and $g_{bb}^{L,R}$ exist [11]. Describing the corresponding Γ_{12}^s in each of our Z' scenario, there are six real free parameters, *i.e.* the complex $g_{sb}^{L,R}$ and the real $g_{\tau\tau}^{L,R}$ ($g_{cc}^{L,R}$) since the diagonal couplings have to be real.

The NP models accommodating the sizable new contribution in Γ_{12}^q suffer from the various experimental bounds, mainly due to the recently updated LHCb data of 1fb^{-1} . In the next section, we analyze the related bounds in detail by focussing on the enhancement of $a_{s\ell}^s$.

III. EXPERIMENTAL CONSTRAINTS

In this section, we analyze the various experimental constraints in obtaining the new sizable contribution to Γ_{12}^s from the $B_s - \bar{B}_s$ mixing. The NP contribution to Γ_{12}^s via the operator $(\bar{s}b)(\bar{f}f)$ where f is a SM fermion can also affect the various B_s or B meson decay processes ⁶. In the Z' models, the new contribution is realized by the tree level FCNC process, which can be large enough to threaten the current experimental bounds. In this section, we introduce the experimental constraints from ΔM_s , $\Delta\Gamma_s$, $\phi_s^{J/\psi\phi}$, $b \rightarrow s\nu\bar{\nu}$, and $B \rightarrow J/\psi K_S$. Then, we will show what extent the NP parameter space explaining the dimuon charge asymmetry can be constrained by such bounds, by applying our Z' scenarios.

For the simplicity, we almost turn off the couplings $g_{\ell\ell}^{L,R}$ for the light leptons $\ell = e^-, \mu^-$ not to consider the tree level NP contribution in the observations such as $B \rightarrow X_s \ell^+ \ell^-$, $B \rightarrow K^* \ell^+ \ell^-$, and $B_s \rightarrow \ell^+ \ell^-$ as shown in [4]. For the case $g_{bb}^{L,R} \neq 0$, a one-loop induced NP

⁵ As a conservative bound, we require the upper limit of the couplings is 0.5 in this paper.

⁶ B generically denotes B_d^0, B_d^\pm mesons.

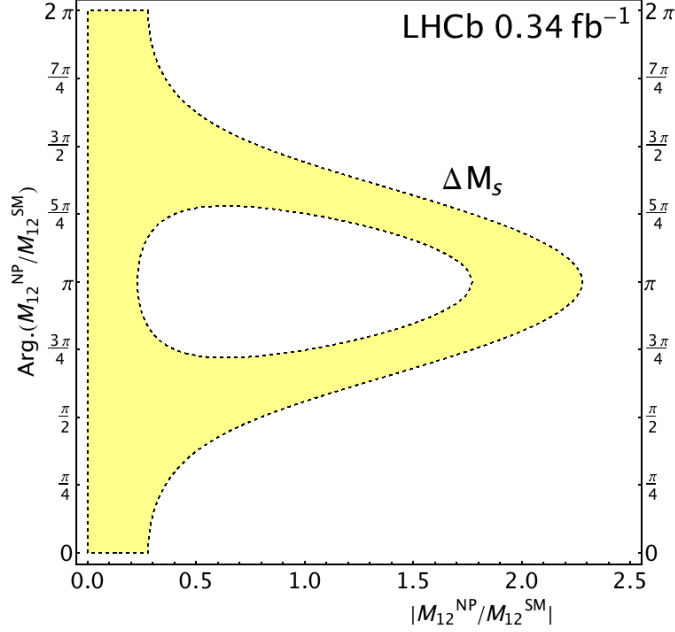


FIG. 2. The yellow colored region denotes the parameter space allowed by the 90% C.L. (1.65σ) experimental bounds of ΔM_s observed at the LHCb 0.34fb^{-1} . The rough upper limit of h_s is 2.3 according to this figure. The results from the CDF and D0 are not so much different from this.

contribution can affect the $b \rightarrow s\gamma$. Such contribution is well summarized in our Appendix A for the future use.

A. ΔM_s

The experimental measurements of ΔM_s both from the LHCb and the Tevatron have no significant deviation from the SM prediction. Therefore, the allowed parameter space is highly constrained as shown in Fig. 2 in terms of the general parameters h_s and $2\sigma_s$. In the SM, the value of M_{12} is obtained dominantly from the box diagram interchanging the W bosons and the t quarks such that [12]

$$M_{12}^{\text{SM}} = \frac{G_F^2}{12\pi^2} M_W^2 (V_{tb} V_{ts}^*) \eta_{2B} f_{B_s}^2 m_{B_s} B_{B_s} S_0(m_t^2/M_W^2), \quad (20)$$

where the loop function $S_0(x) = \frac{4x-11x^2+x^3}{4(1-x)^2} - \frac{3x^3 \log x}{2(1-x)^3}$ and $\eta_{2B} = 0.551$.

With the Z' contribution to the flavor violating interaction $b_{L,R} s_{L,R}$, we obtain the fol-

lowing result from [5, 12, 13]

$$M_{12}^{\text{NP}} = \frac{4G_F}{\sqrt{2}} \frac{1}{g_1^2} \frac{M_Z^2}{M_{Z'}^2} \times \left[\frac{1}{3} \eta^{6/23} (g_{sb}^L)^2 + \frac{1}{3} \eta^{6/23} (g_{sb}^R)^2 - 2 \eta^{3/23} g_{sb}^L g_{sb}^R \left(\frac{1}{4} + \frac{1}{6} \left(\frac{m_{B_s}}{m_b + m_s} \right)^2 \right) \right. \\ \left. + \frac{4}{3} (\eta^{3/23} - \eta^{-24/23}) g_{sb}^L g_{sb}^R \left(\frac{1}{24} + \frac{1}{4} \left(\frac{m_{B_s}}{m_b + m_s} \right)^2 \right) \right] f_{B_s}^2 m_{B_s} B_{B_s} , \quad (21)$$

where $\eta = \alpha_s(M_{Z'})/\alpha_s(m_b)$. Using the value $\alpha_s(M_{Z'} \approx M_Z) \approx 0.118$, $\alpha_s(m_b) \approx 0.22$, $m_t = 172.9$ GeV, $M_W = 80.399$ GeV, $G_F = 1.166 \times 10^{-5}$ GeV⁻², $V_{tb} = 0.88$, and $V_{ts} = 0.0387$ from [14], we obtain

$$h_s = \frac{7.79 \times 10^5}{g_1^2} \times \text{Abs.} \left[(g_{sb}^L)^2 + (g_{sb}^R)^2 - 6 \eta^{-3/23} g_{sb}^L g_{sb}^R \left(\frac{1}{4} + \frac{1}{6} \left(\frac{m_{B_s}}{m_b + m_s} \right)^2 \right) \right. \\ \left. + 4 (\eta^{-3/23} - \eta^{-30/23}) g_{sb}^L g_{sb}^R \left(\frac{1}{24} + \frac{1}{4} \left(\frac{m_{B_s}}{m_b + m_s} \right)^2 \right) \right] \quad (22) \\ = (1.41 \times 10^6) \times \text{Abs.} [(g_{sb}^L)^2 + (g_{sb}^R)^2 - k g_{sb}^L g_{sb}^R] ,$$

where $k \approx 5.33$ is given⁷ and ‘Abs.’ means the absolute value. The value of h_s should be as small as < 2.3 to satisfy the experimental constraint of (16). Therefore, the terms inside the squared bracket of (22) must be as small as $< 1.6 \times 10^{-6}$. This result can be rewritten as

$$\text{Abs.} [(g_{sb}^L)^2 + (g_{sb}^R)^2 - k g_{sb}^L g_{sb}^R] < 1.6 \times 10^{-6} . \quad (23)$$

The quadratic form inside the Abs. symbol of (23) describes a complex hyperbolic surface. With the inclusion of Abs. symbol, the hyperbolic surface is flipped along the asymptotic complex lines satisfying

$$(g_{sb}^L)^2 + (g_{sb}^R)^2 - k g_{sb}^L g_{sb}^R = 0 , \quad (24)$$

or equivalently,

$$g_{sb}^R = a g_{sb}^L , \quad g_{sb}^R = (1/a) g_{sb}^L , \quad (25)$$

where $a \approx 5.135268$. On these asymptotic lines, $\theta_L = \theta_R$ where $\theta_{L,R}$ is the phase of $g_{sb}^{L,R}$ respectively. Consequently, the bound (23) indicate that the generic values of $|g_{sb}^{L,R}|$ must be

⁷ Actually, the coefficients including k is sensitive on our initial choice of the input parameters.

smaller than 10^{-3} unless they are within (or close to) the asymptotic lines (25). Since the ΔM_s constraint parametrized by (23) is highly stringent for $|g_{sb}^{L,R}| > 10^{-3}$, the parameter space containing such values of couplings cannot avoid the fine tuning.

For the case that one of $g_{sb}^{L,R}$ is turned off, we can easily induce that the absolute value of the remaining nonzero coupling must be definitely smaller than 1.8×10^{-3} . Therefore, the required value of $|g_{\tau\tau}^{L,R}|$ or $|g_{cc}^{L,R}|$ for the explanation of the dimuon charge asymmetry in this case must be larger than 1, which is easily induced from analyzing the results in [4, 5].

B. $\Delta\Gamma_s$ and $\phi_s^{J/\psi\phi}$ from $B_s \rightarrow J/\psi\phi$

The enhancement of the like-sign dimuon charge asymmetry is constrained by the experimental measurement of the width difference $\Delta\Gamma_s$ of the mass eigenstate B_s^0 mesons, and the phase difference $\phi_s^{J/\psi\phi}$ between the B_s mixing and the $b \rightarrow sc\bar{c}$ decay. These are simultaneously determined by measuring the indirect CP asymmetry of $B_s \rightarrow J/\psi\phi$ decay. The recent result from the LHCb of 1fb^{-1} integrated luminosity shows that [15]

$$\Delta\Gamma_s = 0.116 \pm 0.018(\text{stat.}) \pm 0.006(\text{syst.}) \text{ ps}^{-1} , \quad (26)$$

$$\phi_s^{J/\psi\phi} = -0.001 \pm 0.101(\text{stat.}) \pm 0.027(\text{syst.}) \text{ rad} , \quad (27)$$

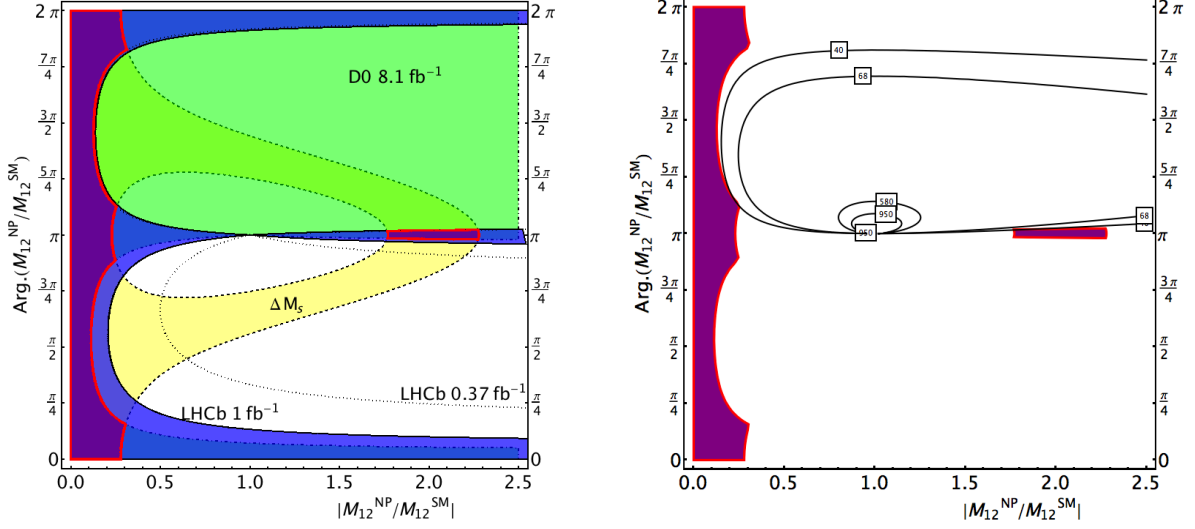
in which $\Delta\Gamma_s$ has about 1.2σ deviation⁸ from $(\Delta\Gamma_s)^{\text{SM}} = (0.087 \pm 0.021) \text{ ps}^{-1}$ and $\phi_s^{J/\psi\phi}$ agrees well with the SM prediction $(\phi_s^{J/\psi\phi})_{\text{SM}} = \text{Arg.} \left((V_{ts}V_{tb}^*)^2 / (V_{cs}V_{cb}^*)^2 \right) = -2\beta_s^{\text{SM}} = -0.036 \pm 0.002$ [3]. Such new LHCb results dramatically reduce the room of new physics contribution in $B_s - \bar{B}_s$ mixing compared to those of the previous LHCb (337 pb^{-1}), the CDF (5.2 fb^{-1}), and the D0 (8.0 fb^{-1}).

We first deal with the issue related with $\phi_s^{J/\psi\phi}$, whose measurement at the LHCb 1fb^{-1} shows the most dramatic changes compared to the previous ones. The analytic expression of $\phi_s^{J/\psi\phi}$ is well summarized in [16] and [5]. Neglecting the SM strong phases in the $B_s \rightarrow J/\psi\phi$ process, we obtain [5, 16]

$$\sin \phi_s^{J/\psi\phi} = \sin(-2\beta_s + \phi_M^s) + 2|r_\lambda| \cos(-2\beta_s + \phi_M^s) \sin \varphi_\lambda , \quad (28)$$

where $\phi_M^s = \text{Arg.}(M_{12}/M_{12}^{\text{SM}})$ is from the NP contribution in the dispersive part of $B_s - \bar{B}_s$ mixing, and the term with r_λ is from the NP contribution in the $b \rightarrow sc\bar{c}$ decay. Note that

⁸ Note that the sign of $\Delta\Gamma_s$ is fixed to be positive in this result.



(a) Experimental bounds in the B_s system

(b) Possible enhancement if $\Gamma_{12}^s = \Gamma_{12}^{s\text{SM}}$

FIG. 3. The experimental bounds apply for the general NP scenarios *without new phases in* $b \rightarrow s\bar{c}\bar{c}$, such as the $g_{\tau\tau}$ scenario. (a) The final allowed region of $h_s = |M_{12}^{\text{NP}}/M_{12}^{\text{SM}}|$ and $2\sigma_s = \text{Arg.}(M_{12}^{\text{NP}}/M_{12}^{\text{SM}})$ from the ΔM_s , $\phi_s^{J/\psi\phi}$ (LHCb 1fb $^{-1}$, 0.37fb $^{-1}$, and D0 8fb $^{-1}$) constraints is shown as the purple color surrounded by the thick red line. The yellow region (inside the dashed line boundary) : allowed by 90% ΔM_s . The green region (inside the dot-dashed line boundary) : allowed by 90% $\phi_s^{J/\psi\phi}$ at the 8.0 fb $^{-1}$ D0. ($\phi_s^{J/\psi\phi} = 0.15 \pm 0.18(\text{stat.}) \pm 0.06(\text{syst.})$ [17]). The blue region (inside the line boundary) : allowed by 90% $\phi_s^{J/\psi\phi}$ at the recent 1.0 fb $^{-1}$ LHCb and the boundary at the 0.37 fb $^{-1}$ at the LHCb in the last year is denoted as the dotted lines. The purple region surrounded by the thick red line denotes the allowed parameter space from all the commented constraints. The mainly remained region is $h_s < 0.3 \ll 1$, which provides a fine tuning choice in the parameter space explaining $a_{s\ell}^s$. The other region of $2\sigma_s \sim \pi$ with $1.7 < h_s < 2.2$ is irrelevant in the enhancement of $a_{s\ell}^s = \text{Im}(\Gamma_{12}^s/M_{12}^s)$ since this region only changes the sign of M_{12}^s respect to its SM value. (b) Without NP contribution to Γ_{12} , we represent the possible enhancement of $-a_{s\ell}^s/(a_{s\ell}^s)^{\text{SM}}$ with the numbers and the contours. In this case, the enhancement is quite limited such that $-a_{s\ell}^s/(a_{s\ell}^s)^{\text{SM}} < 40$ to be consistent with all the experimental bounds.

this result is obtained using the approximation that $|r_\lambda| \ll 1$ from the exact relation in [16]. In the figures to show the allowed parameter space, we use the exact relation.

When there is no NP phase contribution in $b \rightarrow s\bar{c}\bar{c}$, such as $g_{\tau\tau}$ scenario in Z' , we have $r_\lambda = 0$. Since we know that $\sin\phi_M^s = h_s \sin 2\sigma_s / \sqrt{1 + h_s^2 + 2h_s \cos 2\sigma_s} =$

$(h_s \sin 2\sigma_s) \sqrt{\frac{\Delta M_s^{\text{SM}}}{\Delta M_s}} \approx h_s \sin 2\sigma_s$, the small value of $\phi_s^{J/\psi\phi}$ requires $h_s \sin 2\sigma_s$ to be also small. Combining with the ΔM_s constraint, it is possible to show the allowed region in terms of the general parameters h_s and $2\sigma_s$ as Fig. 3. In such cases, the fine tuning $h_s < 0.3 \ll 1$ is required to avoid the constraints from the ΔM_s and $\phi_s^{J/\psi\phi}$ simultaneously. (The region $2\sigma_s \sim \pi$ with $1.7 < h_s < 2.2$ is irrelevant in the enhancement of $a_{s\ell}^s = \text{Im}(\Gamma_{12}^s/M_{12}^s)$ since this only changes the sign of $M_{12}^{s\text{SM}}$.) Without NP contribution to Γ_{12} , the enhancement in $a_{s\ell}^s$ is quite limited such that $-a_{s\ell}^s/(a_{s\ell}^s)^{\text{SM}} < 40$ so that it is impossible to explain the dimuon charge asymmetry within 1σ .

On the other hand, for the cases that we have NP phase contribution in $b \rightarrow sc\bar{c}$, such as g_{cc} scenario in Z' , we have a contribution from $r_\lambda \neq 0$. The NP contribution in the $B_s \rightarrow J/\psi\phi$ amplitude is parametrized as

$$\sum \langle (J/\psi\phi)_\lambda | \mathcal{O}_{\text{NP}} | B_s \rangle = b_\lambda e^{i\varphi_\lambda}, \quad (29)$$

where λ is the polarization of final state vector particles. The longitudinal direction is $\lambda = 0$ and the two transverse directions are $\lambda = \{+, -\}$. The angle ϕ_λ is the new weak phase from the above NP contribution. The ratio of the amplitude $|r_\lambda| = b_\lambda/a_\lambda$ is defined for the SM amplitude a_λ .

In the g_{cc} scenario of Z' model, we obtain the following result according to [16] such that

$$|r_{\lambda=0}| = \left| \frac{1}{g_1^2} \frac{M_Z^2}{M_{Z'}^2} \frac{2(g_{cc}^L + g_{cc}^R)(g_{sb}^L - k_0 g_{sb}^R)}{V_{cb} V_{cs}^* \cdot 0.17} \right|, \quad (30)$$

$$|r_{\lambda=+}| = \left| \frac{1}{g_1^2} \frac{M_Z^2}{M_{Z'}^2} \frac{2(g_{cc}^L + g_{cc}^R)(g_{sb}^L - k_+ g_{sb}^R)}{V_{cb} V_{cs}^* \cdot 0.17} \right|, \quad (31)$$

$$|r_{\lambda=-}| = \left| \frac{1}{g_1^2} \frac{M_Z^2}{M_{Z'}^2} \frac{2(g_{cc}^L + g_{cc}^R)(g_{sb}^L - k_- g_{sb}^R)}{V_{cb} V_{cs}^* \cdot 0.17} \right|, \quad (32)$$

where $k_0 = 1$, $k_+ = 8.8, 9.8$ and $k_- = 0.11, 0.10$ depending on the model of the form factors Melikhov-Stech [18] and Ball-Zwicky [19], respectively.⁹ The vector interaction of the charm quark pair is obtained from the factorization $\langle J/\psi | \bar{c}\gamma^\mu c | 0 \rangle$.

Consequently, we obtain the following expression in the g_{cc} scenario for $|r_\lambda| \ll 1$ and neglecting the SM prediction.

$$\begin{aligned} \sin \phi_s^{J/\psi\phi} = & \frac{h_s \sin 2\sigma_s}{\sqrt{1 + h_s^2 + 2h_s \cos 2\sigma_s}} \\ & + \left| \frac{2}{g_1^2} \frac{M_Z^2}{M_{Z'}^2} \frac{2(g_{cc}^L + g_{cc}^R)(g_{sb}^L - k_{0,\pm} g_{sb}^R)}{V_{cb} V_{cs}^* \cdot 0.17} \right| \frac{1 + h_s \cos 2\sigma_s}{\sqrt{1 + h_s^2 + 2h_s \cos 2\sigma_s}} (\sin \varphi_{0,\pm}). \end{aligned} \quad (33)$$

⁹ Actually, there are typically about 10 % theoretical uncertainties in the form factors. Such consideration in k_+ as an example is shown in our Appendix B.

We first analyze the case $h_s \ll 1$. Then, the above expression becomes

$$\sin \phi_s^{J/\psi \phi} \approx (1.0 \times 10^3) |(g_{cc}^L + g_{cc}^R)(g_{sb}^L - k_{0,\pm} g_{sb}^R)| (\sin \varphi_{0,\pm}) . \quad (34)$$

To satisfy the recent LHCb result of 1fb^{-1} with 90% C.L., we obtain the constraint on the couplings

$$-1.7 \times 10^{-4} < |(g_{cc}^L + g_{cc}^R)(g_{sb}^L - k_{0,\pm} g_{sb}^R)| (\sin \varphi_{0,\pm}) < 1.7 \times 10^{-4} , \quad (35)$$

which provides a strong constraint on the values of $|g_{sb}^{L,R} g_{cc}^{L,R}|$ unless the Z' vector coupling to the charm quark pair is axial. For $|g_{sb}^L| \ll k_+ |g_{sb}^R|$, the most stringent bound is obtained from the $\lambda = +$ case and $|\sin \varphi_+| \approx |\sin \theta_R|$. For the other case, the most stringent bound is obtained from the $\lambda = -$ case and $|\sin \varphi_-| \approx |\sin \theta_L|$. Without considering the (almost) axial vector-like interaction of $Z' c\bar{c}$, the constraint (35) provides

$$\begin{aligned} |g_{sb}^R g_{cc}^{L,R} \sin \theta_R| &< \mathcal{O}(10^{-5}) , \\ |g_{sb}^L g_{cc}^{L,R} \sin \theta_L| &< 10^{-4} . \end{aligned} \quad (36)$$

When $\theta_L = \theta_R$ or $|g_{sb}^L/g_{sb}^R|$ is far from 1, the angle $|\sin(2\tilde{\sigma}_s)|$ is approximately simplified as $|\sin \theta_L|$ or $|\sin \theta_R|$ so that we can directly use the constraint (35) to check the allowed the parameter space for the dimuon charge asymmetry.

On the other case when we have a sizable $h_s > 0.3$, the NP contribution from the mixing and decay of $\phi_s^{J/\psi \phi}$ in (28) can be cancelled to satisfy the strong experimental bound. This is classified by the following cases.

- i) $|g_{sb}^{L,R}| > 10^{-3}$ but $\Gamma_{12}^{\text{NP}}/\Gamma_{12}^{\text{SM}}$ is negligible ¹⁰
- ii) $|g_{sb}^{L,R}| > 10^{-3}$ and $\Gamma_{12}^{\text{NP}}/\Gamma_{12}^{\text{SM}}$ is sizable to enhance $a_{s\ell}^s$
- iii) $|g_{sb}^{L,R}| \leq 10^{-3}$ but $\Gamma_{12}^{\text{NP}}/\Gamma_{12}^{\text{SM}}$ is negligible
- iv) $|g_{sb}^{L,R}| \leq 10^{-3}$ but $\Gamma_{12}^{\text{NP}}/\Gamma_{12}^{\text{SM}}$ is sizable to enhance $a_{s\ell}^s$

For the cases i) and ii), the off-diagonal couplings $g_{sb}^{L,R}$ must satisfy the fine tuning condition (25) due to the ΔM_s constraint. Then, the NP contribution to $\phi_s^{J/\psi \phi}$ by the $b \rightarrow sc\bar{c}$ in (33) is directly constrained by the value of $\sin 2\beta$ from $B^0 \rightarrow J/\psi K_S$ as explained

¹⁰ The coupling $|g_{sb}^{L,R} g_{cc}^{L,R}|$ can be either small or are in a special relation making Γ_{12} small.

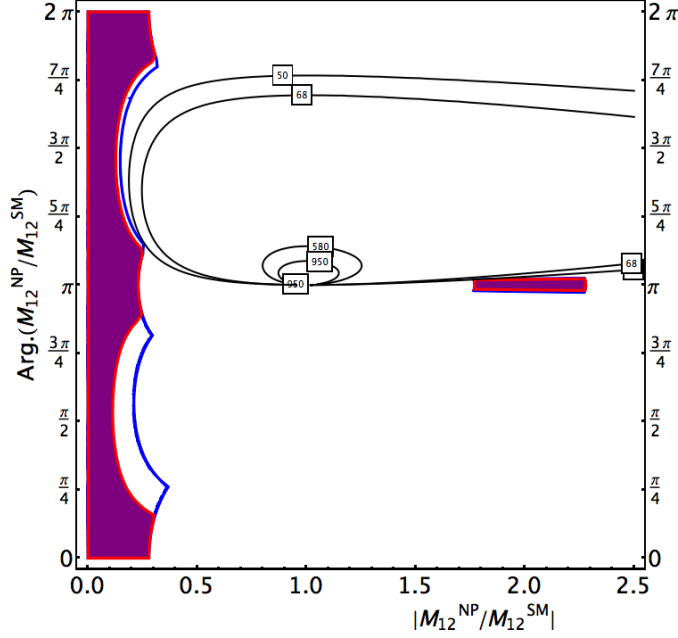


FIG. 4. We represent the allowed parameter space explaining the dimuon charge asymmetry within 1σ for the case i) in the contents. The purple region surrounded by the thick red line is the case without the new phase in $b \rightarrow sc\bar{c}$ as explained in Fig. 3. When h_s is sizable to cancel the contribution from the $b \rightarrow sc\bar{c}$, larger region is allowed by $\phi_s^{J/\psi\phi}$ but the NP parameter space is still constrained by $\sin 2\beta$ as explained in Sec. IIID. The blue line represents the combined bound of ΔM_s , $\phi_s^{J/\psi\phi}$, and $\sin 2\beta$ for the case i). The contours denote the 50, 68, 580, and 950 of the ratio $-a_{s\ell}^s/(a_{s\ell}^s)^{\text{SM}}$. Even with arbitrary contribution in $a_{s\ell}^d$, we see that the combined bound do not allow the enhancement $-a_{s\ell}^s/(a_{s\ell}^s)^{\text{SM}} = 68$ to explain the dimuon charge asymmetry within 1σ .

in Sec. IIID. Considering this effect, it is possible to obtain the limit of the parameters $2\sigma_s$ and h_s for the case i) as shown in Fig. 4. In the figure, the combined bound from ΔM_s , $\phi_s^{J/\psi\phi}$, and $\sin 2\beta$ is represented as the region surrounded by the blue line. In result, it is impossible to obtain the enough enhancement of $a_{s\ell}^s$ to explain the dimuon charge asymmetry within 1σ in case i).

The result of case ii) will not be different from our final result analyzed for $h_s \approx 0$. This is because the $a_{s\ell}^s$ is mainly enhanced by $\Gamma_{12}^{\text{NP}}/\Gamma_{12}^{\text{SM}}$ so that its value is not sensitive to the choice of $g_{sb}^{L,R}$ around the asymptotic lines (25). Since the $a_{s\ell}^s$ of case iv) is also enhanced by $\Gamma_{12}^{\text{NP}}/\Gamma_{12}^{\text{SM}}$, the situation is same for the case iv). From our final result, we need $|g_{cc}^{L,R}| > 1$ for iv), which is unrealistic.

For the case iii), there can be fine tuned region satisfying (27). To obtain $-a_{s\ell}^s/(a_{s\ell}^s)^{\text{SM}} > 68$, the value of $-\sin\phi_M^s = -\text{Arg.}(M_{12}^s/M_{12}^{s\text{SM}})$ must be of order $68(\Delta M_s/\Delta M_s^{\text{SM}})\sin\phi_s^{\text{SM}} \gtrsim 0.2$ from Eq. (15) since $\Gamma_{12}^{\text{NP}}/\Gamma_{12}^{\text{SM}}$ is negligible. To satisfy (27), the value of $\sin\phi_M^s \approx h_s \sin 2\sigma_s$ must be of order $(1.0 \times 10^3)|(g_{cc}^L + g_{cc}^R)(g_{sb}^L - k_\lambda g_{sb}^R)| \sin\varphi_\lambda$, which is at most $|g_{cc}^L + g_{cc}^R| \sin\varphi_\lambda$. Therefore, one of the couplings $|g_{cc}^{L,R}|$ must be at least of order $\mathcal{O}(10^{-1})$. We will see later that the coupling g_{cc}^L of $\mathcal{O}(10^{-1})$ becomes a serious problem in connection with the axial vector solution of g_{cc} couplings to avoid the experimental bounds in the end of Sec. V.¹¹

Now, we move to the issue of $\Delta\Gamma_s$. The analytic expression of $\Delta\Gamma_s/(\Delta\Gamma_s)^{\text{SM}}$ is given as

$$\begin{aligned} \frac{\Delta\Gamma_s}{(\Delta\Gamma_s)^{\text{SM}}} &= \frac{2|\Gamma_{12}| \cos\phi_s}{2|\Gamma_{12}^{\text{SM}}| \cos\phi_s^{\text{SM}}} \\ &= \frac{1}{\sqrt{1+h_s^2+2h_s\cos 2\sigma_s}} \left[(1+h_s\cos 2\sigma_s)(1+\tilde{h}_s\cos 2\tilde{\sigma}_s) + h_s\tilde{h}_s\sin 2\sigma_s\sin 2\tilde{\sigma}_s \right. \\ &\quad \left. - \tan\phi_s^{\text{SM}} \left(h_s\sin 2\sigma_s(1+\tilde{h}_s\cos 2\tilde{\sigma}_s) - \tilde{h}_s\sin 2\tilde{\sigma}_s(1+h_s\cos 2\sigma_s) \right) \right]. \end{aligned} \quad (37)$$

With Eq. (19), we can see that the enhancement of dimuon charge asymmetry is always possible without suffering from the constraint on $\Delta\Gamma_s/(\Delta\Gamma_s)^{\text{SM}}$. This is because the enhancement of $a_{q\ell}$ is from $\text{Im}(\Gamma_{12})$ and that of $\Delta\Gamma_q$ from $\text{Re}(\Gamma_{12})$ along the direction of $\text{Re}(M_{12})$, as easily expected from the first relation in (15). The consistent parameter space is shown with 2D plot as our Fig. 5, where the parameter space is free from the ΔM_s bound.

On the other hand, the other constraints from [20] such as $B^+ \rightarrow K^+\tau^+\tau^-$, $B_s \rightarrow \tau^+\tau^-$, $B \rightarrow X_s\tau^+\tau^-$, $B \rightarrow X_s\gamma$, $B \rightarrow X_s\ell^+\ell^-$, and $B \rightarrow K^{(*)}\ell^+\ell^-$ provide additional interesting limit in the allowed parameter space. (Among them, the strongest bound is given by $B^+ \rightarrow K^+\tau^+\tau^-$.) The experimental bounds can be analytically expressed with $\tilde{h}_s\cos 2\tilde{\sigma}_s$ and $\tilde{h}_s\sin 2\tilde{\sigma}_s$, in addition to the dimuon charge asymmetry value in (45). The bound is $|\Gamma_{12}^{s\text{NP}}/\Gamma_{12}^{s\text{SM}}| < 0.3$ from [20]. Therefore, it is possible to check the consistency of $a_{s\ell}^s$, $\Delta\Gamma_s$, and $B^+ \rightarrow K^+\tau^+\tau^-$ in terms of such parameters as Fig. 5. Consequently, the three experimental results are only marginally consistent at the region allowing large NP contribution in $a_{s\ell}^d$.

¹¹ When $\theta_L \approx \theta_R$ or $|g_{sb}^L/g_{sb}^R|$ is far from 1, the result will be same as that of our case i).

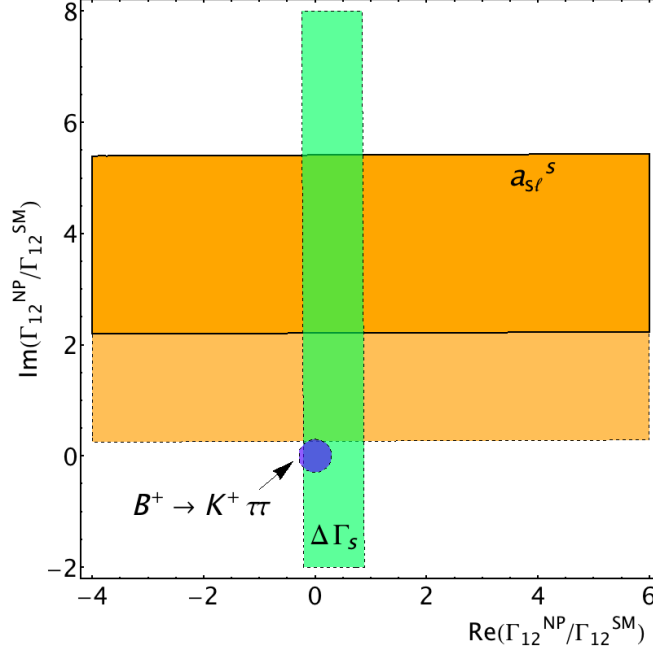


FIG. 5. This shows the consistency of explaining the observed $a_{s\ell}^s$ within 1σ . The orange color with thick line boundary region denotes $-a_{s\ell}^s/(a_{s\ell}^s)^{\text{SM}} > 580$ and the dashed line 68 when $h_s = |M_{12}^{\text{NP}}/M_{12}^{\text{SM}}| \ll 1$ such as the $g_{\tau\tau}$ scenario. The experimental results with 90%C.L. $\Delta\Gamma_s$ at the LHCb 1fb^{-1} is shown with light green color, while the result of $B^+ \rightarrow K^+ \tau^+ \tau^-$ from [20] is shown in the light purple color. Actually this bound also covers other bounds such as $B_s \rightarrow \tau^+ \tau^-$, $B \rightarrow X_s \tau^+ \tau^-$, $B \rightarrow X_s \gamma$, $B \rightarrow X_s \ell^+ \ell^-$, and $B \rightarrow K^{(*)} \ell^+ \ell^-$. (Among them, the strongest bound is given by $B^+ \rightarrow K^+ \tau^+ \tau^-$ as seen in [20].) Figure is simply depicted in terms of $\text{Re}(\Gamma_{12}^{\text{NP}}/\Gamma_{12}^{\text{SM}}) = \tilde{h}_s \cos 2\tilde{\sigma}_s$ and $\text{Im}(\Gamma_{12}^{\text{NP}}/\Gamma_{12}^{\text{SM}}) = \tilde{h}_s \sin 2\tilde{\sigma}_s$ with the assumption that $h_s \ll 1$. We can easily see that the explanation of $a_{s\ell}^s$ and the experimental bound $\Delta\Gamma_s$ are orthogonal since they depend on the $\text{Im}(\Gamma_{12}^{\text{NP}})$ and $\text{Re}(\Gamma_{12}^{\text{NP}})$, respectively. The three experimental results are only marginally consistent.

C. $b \rightarrow s\nu\bar{\nu}$

In the case that the non-zero $g_{sb}^{L,R} g_{\tau\tau}^L$ provides the sizable enhancement in $a_{s\ell}^s$, the coupling $g_{\tau\tau}^L$ is constrained by its partner in the SU(2) doublet $g_{\nu\nu}^L \equiv g_{\nu\nu}$. Following the analysis in [21, 22], we can obtain the limit of $g_{\nu\nu} g_{sb}^{L,R}$ from $B \rightarrow K^* \nu\bar{\nu}$, $B \rightarrow K \nu\bar{\nu}$, and $B \rightarrow X_s \nu\bar{\nu}$. The detail way of calculating the Z' contribution in these processes are well summarized in our Appendix C.

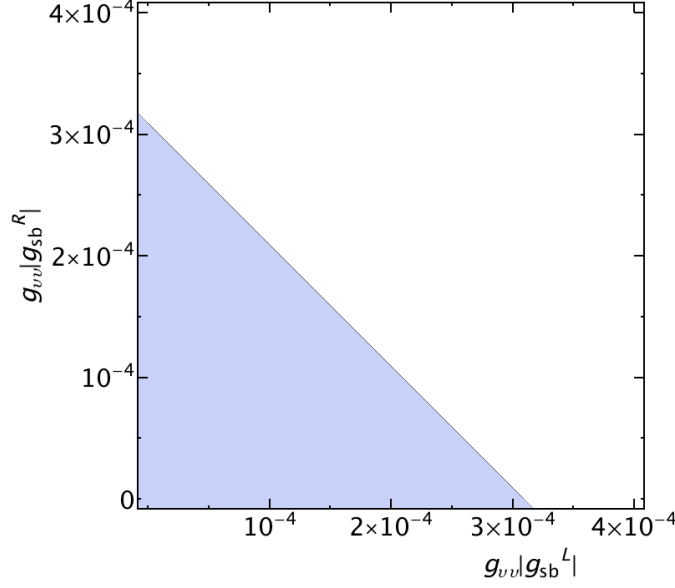


FIG. 6. The colored region denotes the parameter space allowed by the 90% C.L. experimental bounds of $g_{\nu\nu}|g_{sb}^{L,R}|$. This is the case that $\theta_L = \theta_R \equiv \theta = \pi/4$ and $g_{\nu\nu} > 0$. This parameter space is free from the $\Delta\Gamma_s$ bound by making $\Gamma_{12}^{s\text{NP}}/\Gamma_{12}^{s\text{SM}}$ almost imaginary, as well as the ΔM_s bound. Since $g_{\tau\tau}^L = g_{\nu\nu}$, the rough upper limit of the coupling is obtained $g_{\tau\tau}^L|g_{sb}^{L,R}| \lesssim 3 \times 10^{-4}$. Even for the other cases, the upper limit is below 10^{-3} .

As experimental upper bounds at 90% C.L. (1.65σ), we obtain from [14, 23] such that

$$\text{Br}(B \rightarrow K^* \nu \bar{\nu}) < 8 \times 10^{-5} \quad [14] , \quad (38)$$

$$\text{Br}(B \rightarrow K \nu \bar{\nu}) < 1.3 \times 10^{-5} \quad [14] , \quad (39)$$

$$\text{Br}(B \rightarrow X_s \nu \bar{\nu}) < 6.4 \times 10^{-4} \quad [23] . \quad (40)$$

Combining all the limits, we obtain the limit of the couplings as Fig. 6. The allowed range of $g_{\nu\nu}|g_{sb}^{L,R}|$ from the 90% C.L. experimental bounds is shown. We deal with the case that $\theta_L = \theta_R \equiv \theta$, which is considered in the fine-tuned region of (25). This figure is an example $\theta = \pi/4$ and $g_{\nu\nu} > 0$. The rough upper limit of the coupling is obtained $g_{\nu\nu}|g_{sb}^{L,R}| < 3 \times 10^{-4}$. Even for the other cases, the upper limit is below 10^{-3} .

In the $g_{\tau\tau}^L$ scenario, this provides a strong direct upper bound of the couplings as shown in Fig. 7. To explain the asymmetry within 1σ , the value of $|g_{\tau\tau}^R|$ must be much larger than that of $|g_{\tau\tau}^L|$.¹²

¹² In this case, the anomaly cancellation in the $g_{\tau\tau}$ scenario is threaten, unless we assume a scenario like

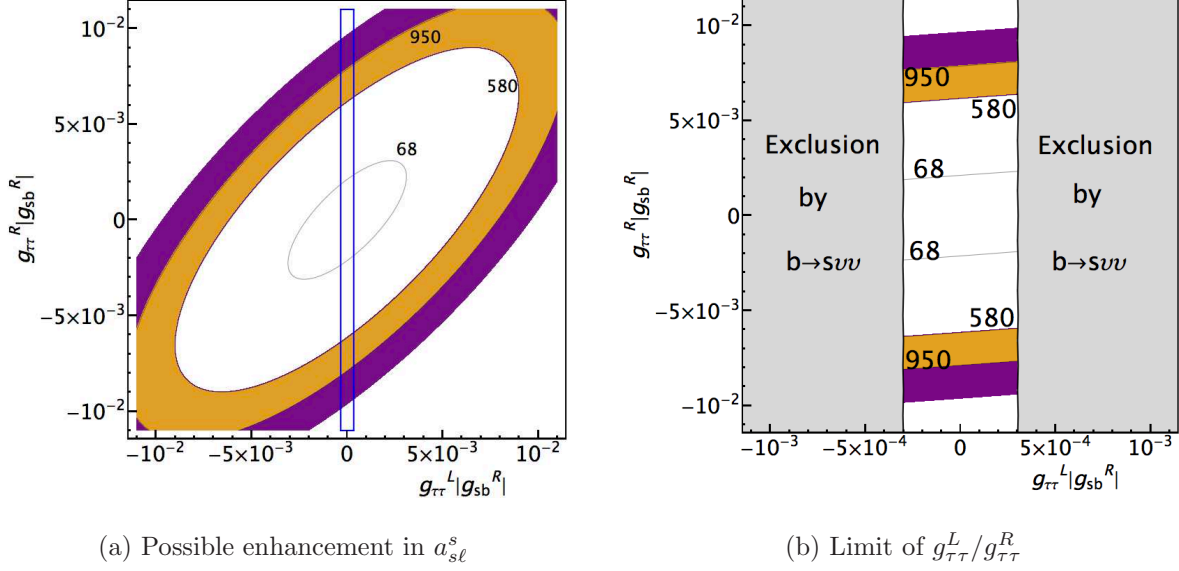


FIG. 7. The limit of the couplings explaining the observed $a_{s\ell}^s$ in the $g_{\tau\tau}$ scenario is shown. In (a), the region inside the blue line box is those remained after applying the $b \rightarrow s\nu\bar{\nu}$ constraint, which is precisely shown in (b). In figure (b), we expressed the conservative exclusion region (grey region) based on the experimental bounds of 90% C.L from the $b \rightarrow s\nu\bar{\nu}$ processes, which is $|g_{\tau\tau}^L g_{sb}^{L,R}| < 3 \times 10^{-4}$. This is the fine-tuned case that $g_{sb}^R = a g_{sb}^L$ and $\theta_L = \theta_R = \pi/4$ as an example. This parameter space is free from the $\Delta\Gamma_s$ bound by making $\Gamma_{12}^{s\text{NP}}/\Gamma_{12}^{s\text{SM}}$ almost imaginary, as well as the ΔM_s bound. The ratio of $-a_{s\ell}^s/(a_{s\ell}^s)$ is shown as a contour plot with the contours 68, 580, and 950. To explain the asymmetry within 1σ , the value of $|g_{\tau\tau}^R|$ must be much larger than $|g_{\tau\tau}^L|$.

D. $\sin 2\beta$ from $B^0 \rightarrow J/\psi K_S$

In this section, we deal with the additional experimental bound when the NP phases contribute to the $b \rightarrow scc$ process, such as the g_{cc} scenario. This is the indirect CP asymmetry $\sin 2\beta$ in the “golden plate” mode $B \rightarrow J/\psi K_S$. The SM prediction of $\sin 2\beta$ can be obtained from the fit of the unitarity triangle. According to [25], we obtain $\sin(2\beta)^{\text{fit}} = 0.731 \pm 0.038$, while the experimental measurements provide $\sin 2\beta^{\text{meas}} = 0.668 \pm 0.028$. In this case, the SM prediction is within 1σ of the measured value. The detail analytic form of $\sin 2\beta$ is well described in [16] and [5], which is similar to $\sin 2\beta_s$ in $B_s \rightarrow J/\psi \phi$ as (28). In the absence

the effective Z' model [24]. This is because there is no way to cancel the $\text{SU}(2)^2\text{U}(1)'$ anomaly from the $g_{\tau\tau}^R$ coupling.

of the SM strong phase,

$$\sin 2\beta^{\text{meas}} = \sin(2\beta)^{\text{fit}} + 2|r| \cos(2\beta)^{\text{fit}} \sin \varphi . \quad (41)$$

As (28), this relation is obtained when $|r| \ll 1$ and we use the exact relation in [16] in our figures.

In the g_{cc} *scenario*, the analytic form of $|r|$ is obtained as

$$|r| = \left| \frac{1}{g_1^2} \frac{M_Z^2}{M_{Z'}^2} \frac{2(g_{cc}^L + g_{cc}^R)(g_{sb}^L + g_{sb}^R)}{V_{cb}V_{cs}^* \cdot 0.17} \right| \approx (5.2 \times 10^2) \times |(g_{cc}^L + g_{cc}^R)(g_{sb}^L + g_{sb}^R)| , \quad (42)$$

and the angle φ is simply obtained in the fine-tuned case (25) such that $\varphi = \theta, \theta + \pi$. Therefore, the allowed range with 90% C.L. of the experimental result and the SM fit is obtained as

$$-1.4 \times 10^{-4} < |(g_{cc}^L + g_{cc}^R)(g_{sb}^L + g_{sb}^R)| \sin \varphi < 1.4 \times 10^{-5} . \quad (43)$$

As the experimental bound by $\phi_s^{J/\psi\phi}$, this provides the strong constraint on the NP parameter space unless the coupling $Z'c\bar{c}$ is (almost) axial vector-like. This bound will be shown in Sec. V with other experimental constraints.

On the other hand, the fitting value of $\sin(2\beta)^{\text{fit}}$ is enlarged if we drop the value of $|V_{ub}|$ as an input since its inclusive and exclusive determination has a large difference. Instead, it is possible to use as inputs from the experiments, ϵ_K , $\Delta M_s/\Delta M_d$, $\text{Br.}(B \rightarrow \tau\nu)$. In this case, we obtain $\sin(2\beta)^{\text{fit}} = 0.867 \pm 0.048$ which induces more than 3σ deviation from the observed central value [26]. By doing this, we can accommodate sizable NP contribution to $\sin 2\beta$ by $g_{sb}^{L,R}g_{cc}^{L,R}$ without sizable deviations in the $B \rightarrow \tau\nu$ branching ratio and ϵ_K . In this case, the value of $|r|$ from the NP contribution is allowed up to $20.0 + 6.5 = 26.5$ % with the 1σ predictions. In terms of the g_{cc} *scenario*, the allowed range with 90% C.L. of the experimental result and the SM fit in this case induces

$$-2.8 \times 10^{-4} < |(g_{cc}^L + g_{cc}^R)(g_{sb}^L + g_{sb}^R)| \sin \varphi < -1.0 \times 10^{-4} . \quad (44)$$

The corresponding parameter region will be discussed in Sec. V.

IV. $g_{\tau\tau}$ SCENARIO FOR THE DIMUON CHARGE ASYMMETRY

In this section, we explore the possible parameter space of the $g_{\tau\tau}$ *scenario* to explain the like-sign dimuon charge asymmetry, combined with the experimental bounds discussed

in the previous section. In this scenario, the enhancement of Γ_{12}^2 is realized in the process of the τ loop-induced Z' exchange. As seen in Fig. 3, we can simply assume $h_s \ll 1$ for the rough analysis. Then, the ratio of the flavor specific asymmetry

$$\begin{aligned} a_{s\ell}^s/(a_{s\ell}^s)^{\text{SM}} &= -\tilde{h}_s \sin 2\tilde{\sigma}_s \cot \phi_s^{\text{SM}} + 1 + \tilde{h}_s \cos 2\tilde{\sigma}_s \\ &\approx -(2.6 \times 10^2) \tilde{h}_s \sin 2\tilde{\sigma}_s + 1 + \tilde{h}_s \cos 2\tilde{\sigma}_s, \end{aligned} \quad (45)$$

where we put the central value of $\phi_s^{\text{SM}} = 3.8 \times 10^{-3}$. Due to the strong LHCb constraint on $\Delta\Gamma_s$, the term $-(2.6 \times 10^2) \tilde{h}_s \sin 2\tilde{\sigma}$ is dominant so that $\sin 2\tilde{\sigma}_s$ is far from 0. The value of \tilde{h}_s in the $g_{\tau\tau}$ scenario is obtained from [5] such that

$$\begin{aligned} \tilde{h}_s &\approx (6.7 \times 10^3) \times \text{Abs.} \left[((g_{sb}^L)^2 + (g_{sb}^R)^2) \{ 1.1 g_{\tau\tau}^L g_{\tau\tau}^R - 0.5((g_{\tau\tau}^L)^2 + (g_{\tau\tau}^R)^2) \} \right. \\ &\quad \left. + g_{sb}^L g_{sb}^R \{ -3.3 g_{\tau\tau}^L g_{\tau\tau}^R + 1.0((g_{\tau\tau}^L)^2 + (g_{\tau\tau}^R)^2) \} \right]. \end{aligned} \quad (46)$$

To obtain the enhancement in $a_{s\ell}^s$ as large as our second reference point $(1, -580)$ in (10), the rough lower limit of the couplings inside the Abs. symbol must be $3.3 \times 10^{-4} = (1.8 \times 10^{-2})^2$ to for $\sin 2\tilde{\sigma}_s = 1$. To obtain the enhancement as our first reference point $(a_{s\ell}^d/(a_{s\ell}^d)^{\text{SM}}, a_{s\ell}^s/(a_{s\ell}^s)^{\text{SM}}) = (21, -68)$, the limit lowers to $3.9 \times 10^{-5} = (6.2 \times 10^{-3})^2$. Consequently, we roughly obtain the limit of the dominant new coupling to explain the dimuon charge asymmetry within 1σ in the χ^2 -fit

$$\begin{aligned} |g_{sb}^{L,R} g_{\tau\tau}^{L,R}| &> 1.8 \times 10^{-2} \text{ without } (a_{s\ell}^d)^{\text{NP}}, \\ |g_{sb}^{L,R} g_{\tau\tau}^{L,R}| &> 6.2 \times 10^{-3} \text{ with } a_{s\ell}^d/(a_{s\ell}^d)^{\text{SM}} = 21. \end{aligned} \quad (47)$$

Since $|g_{\tau\tau}^{L,R}| < 1$, the values of $\text{Max}\{|g_{sb}^{L,R}|\}$ cannot be smaller than $\sim 6.2 \times 10^{-3}$ so that the couplings $g_{sb}^{L,R}$ lie on the asymptotic lines (25), having more than 1% fine tuning. The allowed parameter space is shown in Fig. 8 where we used $g_{\tau\tau}^L = 0.1 g_{\tau\tau}^R$ to maximally satisfy the constraint by $b \rightarrow s\nu\bar{\nu}$ as explained in Sec. III C. We see that the rough consistent region of $|g_{sb}^R g_{\tau\tau}^R|$ is about 10^{-2} with $a_{s\ell}^d/(a_{s\ell}^d)^{\text{SM}} = 21$. We also show the allowed parameter space of $\Delta\Gamma_s$ and $B^+ \rightarrow K^+ \tau^+ \tau^-$ from [20], redrawn from the allowed region in Fig. 5.

Consequently, the $g_{\tau\tau}$ scenario where the Z' coupling to the τ pair enhances the $a_{s\ell}^s$ requires the existence of the coupling $|g_{sb}^{L,R} g_{\tau\tau}^{L,R}|$ larger than about 10^{-2} to explain the dimuon charge asymmetry. Therefore, this parameter space cannot avoid the fine tuning from the ΔM_s constraint. In addition, due to the constraint from the $b \rightarrow s\nu\bar{\nu}$ experiments, the coupling $|g_{\tau\tau}^L|$ must be as small as 3×10^{-4} . This result demands a non-trivial approach

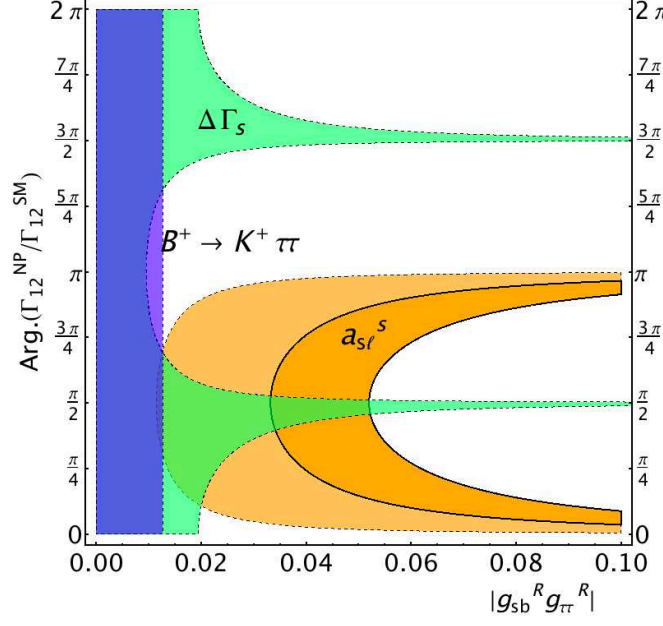


FIG. 8. We changed the parameters in Fig. 5 in terms of $2\tilde{\sigma}_s - |g_{sb}^R g_{\tau\tau}^R|$ in the conservative case that $g_{\tau\tau}^L = 0.1g_{\tau\tau}^R$ and $g_{sb}^R = ag_{sb}^L$ ($h_s \approx 0$). The description on the colored region is same as that in Fig. 5. This shows better understanding on the limits of the couplings in the $g_{\tau\tau}$ scenario. We see that the rough consistent region of $|g_{sb}^R g_{\tau\tau}^R|$ is about 10^{-2} with $a_{s\ell}^d/(a_{s\ell}^d)^{\text{SM}} = 21$.

in establishing an anomaly free model as mentioned at the end of Sec. IIIC. The allowed parameter space explaining the observed $a_{s\ell}^s$ within 1σ is marginally consistent with the experimental bounds of $\Delta\Gamma_s$ at the LHCb 1fb^{-1} and the result of $B^+ \rightarrow K^+ \tau^+ \tau^-$ from [20].

V. g_{cc} SCENARIO

In this section, we explore the possible parameter space of the g_{cc} scenario to explain the like-sign dimuon charge asymmetry, combined with the experimental bounds discussed in the Sec. III. The enhancement of Γ_{12}^s from the interference of the SM process and the Z' induced tree level FCNC in $b \rightarrow sc\bar{c}$ is calculated from [27, 28] such that

$$\begin{aligned} \Gamma_{12}^{\text{SM}+Z'} = & -\frac{m_b^2}{3\pi(2m_{B_s})} G_F^2 V_{cb} V_{cs}^* \frac{1}{g_1^2} \frac{M_Z^2}{M_{Z'}^2} K_1 \sqrt{1-4x_c} \\ & \times \left[4g_{sb}^L g_{cc}^L \left\{ (1-x_c) \langle \mathcal{O}_{LL} \rangle + (1+2x_c) \langle \tilde{\mathcal{O}}_{RR} \rangle \right\} \right. \\ & + 4g_{sb}^R g_{cc}^L \left\{ (1-x_c) \langle \mathcal{O}_{LR} \rangle + (1+2x_c) \langle \tilde{\mathcal{O}}_{RL} \rangle \right\} \\ & \left. + 12x_c g_{sb}^L g_{cc}^R \langle \mathcal{O}_{LL} \rangle + 12x_c g_{sb}^R g_{cc}^R \langle \mathcal{O}_{LR} \rangle \right] , \end{aligned} \quad (48)$$

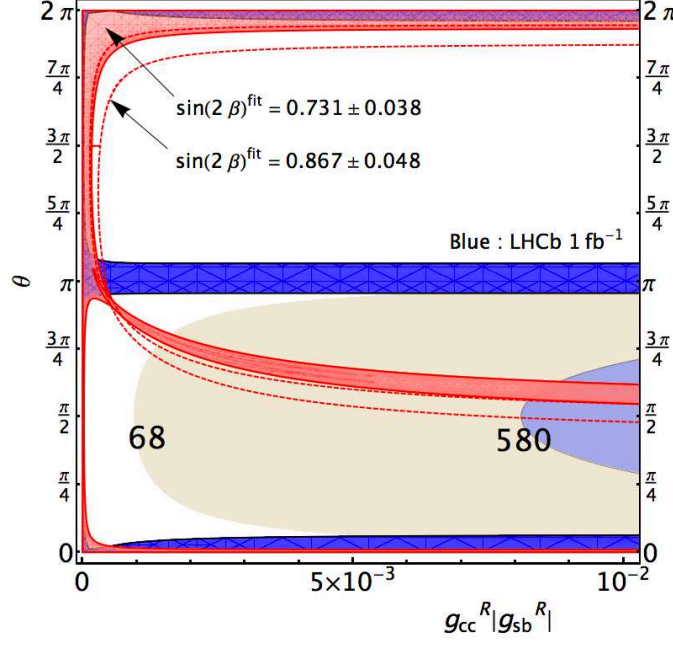


FIG. 9. We represent the allowed parameter space explaining the dimuon charge asymmetry by fixing $g_{cc}^L = 0$ and $g_{cc}^R > 0$ on the fine tuning region $g_{sb}^R = a g_{sb}^L$. (Therefore, $\theta_L = \theta_R = \theta$.) The parameter region $g_{cc}^R |g_{sb}^R| > 10^{-2}$ is not considered to avoid the rough constraint from $\bar{B}^0 \rightarrow D^+ D_s^-$ [29]. Even though we allow the NP contribution which is about half of the SM tree level prediction, it is roughly $g_{cc}^R |g_{sb}^R| / g_1^2 < 0.5 |V_{cb} V_{cs}^*| \sim 0.02$. The numbers in the contours denote the ratio $-a_{s\ell}^s / (a_{s\ell}^s)^{\text{SM}}$ as previous figures. The light pink region denotes the 90% bound from the $B^0 \rightarrow J/\psi K_S$ considering the usual fit $\sin(2\beta)^{\text{fit}} = 0.731 \pm 0.038$ and the area surrounded by the red dashed line is for the special fit $\sin(2\beta)^{\text{fit}} = 0.867 \pm 0.048$ in [26]. The blue region is 90% of $\phi_s^{J/\psi\phi}$ at the recent 1.0 fb^{-1} LHCb. The minimum value of $|g_{cc}^R g_{sb}^R|$ to explain the D^0 dimuon charge asymmetry within 1σ is about 8×10^{-3} and 10^{-3} , without the NP contribution to $a_{s\ell}^d$ and with the maximal contribution of $a_{s\ell}^d / (a_{s\ell}^d)^{\text{SM}} = 21$, respectively. These bounds do not satisfy the experimental constraints, which is expected in our simple analysis.

where $x_c \equiv m_c^2/m_b^2$ and $K_1 = 3.11$ is calculated from the Wilson coefficient of the corresponding operators as in [27, 28]. The hadronic matrix elements are given as

$$\begin{aligned}
\langle \mathcal{O}_{LL} \rangle &\equiv \langle B_s | (\bar{s}_L \gamma_\mu b_L) (\bar{s}_L \gamma^\mu b_L) | \bar{B}_s \rangle = \frac{2}{3} m_{B_s}^2 f_{B_s}^2 B_1 , \\
\langle \tilde{\mathcal{O}}_{RR} \rangle &\equiv \langle B_s | (\bar{s}_L b_R) (\bar{s}_L b_R) | \bar{B}_s \rangle = -\frac{5}{12} m_{B_s}^2 f_{B_s}^2 \left(\frac{m_{B_s}}{m_b + m_s} \right)^2 B_2 , \\
\langle \mathcal{O}_{LR} \rangle &\equiv -2 \left[\frac{1}{4} + \frac{1}{6} \left(\frac{m_{B_s}}{m_b + m_s} \right)^2 \right] m_{B_s}^2 f_{B_s}^2 B_3 , \\
\langle \tilde{\mathcal{O}}_{RL} \rangle &\equiv 2 \left[\frac{1}{24} + \frac{1}{4} \left(\frac{m_{B_s}}{m_b + m_s} \right)^2 \right] m_{B_s}^2 f_{B_s}^2 B_4 ,
\end{aligned} \tag{49}$$

where B_1, B_2, B_3, B_4 are the bag parameters, and $f_{B_s} = (238.8 \pm 9.5)$ MeV. This result is different from that [5] especially adding the suppression factor x_c at the coefficient of the contribution by $g_{sb}^R g_{cc}^R$.

The value of \tilde{h}_s in the g_{cc} scenario is obtained such that

$$\tilde{h}_s \approx 173.7 \times \left| (1.15 g_{sb}^L - 1.76 g_{sb}^R) g_{cc}^R + (-1.03 g_{sb}^L + 0.64 g_{sb}^R) g_{cc}^L \right| . \tag{50}$$

When $h_s \ll 1$, the ratio of the flavor specific asymmetry is

$$a_{s\ell}^s / (a_{s\ell}^s)^{\text{SM}} \approx -4.6 \times 10^4 \times \left| (1.15 g_{sb}^L - 1.76 g_{sb}^R) g_{cc}^R + (-1.03 g_{sb}^L + 0.64 g_{sb}^R) g_{cc}^L \right| \sin 2\tilde{\sigma}_s , \tag{51}$$

in the region that the contribution from $\text{Re}(\Gamma_{12}^{s\text{NP}}/\Gamma_{12}^{s\text{SM}})$ is suppressed to avoid the $\Delta\Gamma_s$ bound. Then, we directly obtain the rough lower limit of the couplings from (51). To obtain the dimuon charge asymmetry within 1σ without any NP contribution in $a_{s\ell}^d$, we have

$$\left| (1.15 g_{sb}^L - 1.76 g_{sb}^R) g_{cc}^R + (-1.03 g_{sb}^L + 0.64 g_{sb}^R) g_{cc}^L \right| \cdot |\sin \theta_{L(R)}| > 1.3 \times 10^{-2} , \tag{52}$$

while for $(a_{s\ell}^d / (a_{s\ell}^d)^{\text{SM}}, a_{s\ell}^s / (a_{s\ell}^s)^{\text{SM}}) = (21, -68)$, we have

$$\left| (1.15 g_{sb}^L - 1.76 g_{sb}^R) g_{cc}^R + (-1.03 g_{sb}^L + 0.64 g_{sb}^R) g_{cc}^L \right| \cdot |\sin \theta_{L(R)}| > 1.4 \times 10^{-3} . \tag{53}$$

Consequently, we roughly obtain the limit of the dominant new coupling to explain the dimuon charge asymmetry within 1σ in the χ^2 -fit

$$\begin{aligned}
|g_{sb}^{L,R} g_{cc}^{L,R} \sin \theta_{L(R)}| &> 10^{-2} \text{ without } (a_{s\ell}^d)^{\text{NP}} , \\
|g_{sb}^{L,R} g_{cc}^{L,R} \sin \theta_{L(R)}| &> 10^{-3} \text{ with } a_{s\ell}^d / (a_{s\ell}^d)^{\text{SM}} = 21 .
\end{aligned} \tag{54}$$

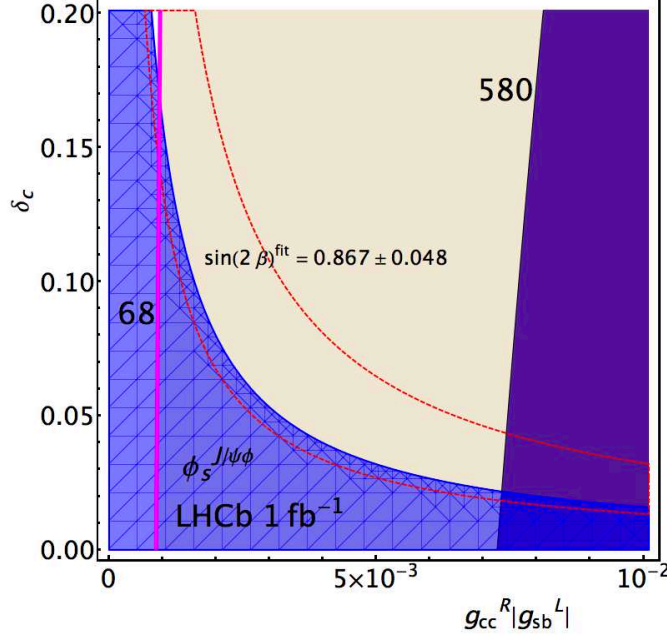


FIG. 10. We show what extent the interaction $Z'c\bar{c}$ should be axial vector-like in this figure. For various values of the difference $\delta_c \equiv (g_{cc}^L + g_{cc}^R)/g_{cc}^R$, our parameter space explaining the dimoun charge asymmetry is shown for $\delta_c > 0$, by fixing $g_{sb}^R \approx (1/a)g_{sb}^L$ with $\theta_L = \theta_R = 3\pi/2$, which is different from the case in Fig. 9. The numbers in the contours denote the value of the ratio $-a_{s\ell}^s/(a_{s\ell}^s)^{\text{SM}}$. The contour line with pink color is the boundary $-a_{s\ell}^s/(a_{s\ell}^s)^{\text{SM}} = 68$ which demand $a_{s\ell}^d/(a_{s\ell}^d)^{\text{SM}} = 21$ to explain the dimoun charge asymmetry within 1σ in the fit of Fig. 1. The meshed blue region denotes the 90% allowed region by the recent LHCb 1fb^{-1} result of $\phi_s^{J/\psi\phi}$ and the area surrounded by the red dash line is that explaining the $\sin 2\beta$ with the special fit $\sin(2\beta)^{\text{fit}} = 0.867 \pm 0.048$ proposed in [26]. Of course, all the blue region of $\phi_s^{J/\psi\phi}$ is also allowed by that using the usual fit $\sin(2\beta)^{\text{fit}} = 0.731 \pm 0.038$. In this case, the coupling $|g_{cc}^R g_{sb}^R| > 7.5 \times 10^{-3}$ and 10^{-3} are required for the explanation of the asymmetry within 1σ without the NP contribution to $a_{s\ell}^d$ and with the maximal contribution of $a_{s\ell}^d/(a_{s\ell}^d)^{\text{SM}} = 21$, respectively. Our parameter space with $-a_{s\ell}^s/(a_{s\ell}^s)^{\text{SM}} > 580$ and $a_{s\ell}^d/(a_{s\ell}^d)^{\text{SM}} = 1$ can simultaneously explain the recent LHCb 1fb^{-1} result and the $\sin 2\beta$ for $\delta_c < 2.5 \times 10^{-2}$.

In this case, the magnitude of $|g_{sb}^{L,R}|$ has less fine tuning from the ΔM_s constraint compared to that in the $g_{\tau\tau}$ scenario. Unless the interaction $Z'c\bar{c}$ is (almost) axial vector-like, the result (54) shows a direct contradiction with the constraint by $\phi_s^{J/\psi\phi}$ we obtained in (36), as well as the $\sin 2\beta$ measurements in Sec. IIID. This result is shown in Fig. 9 in the simple

case $g_{cc}^L = 0$ and $g_{sb}^R = ag_{sb}^L$.

When $|g_{cc}^L + g_{cc}^R| \ll 1$, the constraint by the $\phi_s^{J/\psi\phi}$ at the 1.0 fb^{-1} LHCb is loosen. We show what extent the interaction $Z'c\bar{c}$ should be axial vector-like in our Fig. 10, simultaneously explaining the interesting parameter region of $\sin 2\beta$ using $\sin(2\beta)^{\text{fit}} = 0.867 \pm 0.048$ [26]. As a result, for the explanation of the asymmetry within 1σ without the NP contribution to $a_{s\ell}^d$, we can find the consistent parameter space $|g_{cc}^R g_{sb}^R| > 7.5 \times 10^{-3}$ and $\delta_c < 2.5 \times 10^{-2}$ when $g_{sb}^R = ag_{sb}^L$ with $\theta_L = \theta_R = 3\pi/2$.

Finally, we discuss the possibility of the model construction providing the (almost) axial vector-like interaction $Z'c\bar{c}$. In this case, we need the sizable coupling $|g_{cc}^L| \sim |g_{cc}^R|$ at least $\mathcal{O}(10^{-1})$ not to make the fine tuning of $g_{sb}^{L,R}$ from the ΔM_s worse. Since the left-handed charm quark constitutes a SU(2) doublet with the left-handed strange quark, we also need the sizable g_{ss}^L of $\mathcal{O}(10^{-1})$. If we do not have the equally sizable couplings g_{uu}^L and g_{dd}^L , we automatically obtain the off-diagonal couplings g_{uc}^L and g_{ds}^L . However, the existence of such off-diagonal couplings suffer from the experimental constraints such as K or D meson mixings. For example, the latter process provides the strong upper limit of the g_{uc}^L coupling as small as 2×10^{-4} [30, 31]. Considering the CKM relation of $g_{uc}^L \approx 0.23g_{cc}^{L,R}$, the coupling $|g_{cc}^{L,R}|$ must be smaller than 10^{-3} , which in turn demands $|g_{sb}^{L,R}g_{cc}^{L,R}| < 10^{-3}$. This is out of the 1σ region for the dimuon charge asymmetry even with arbitrary contribution in $a_{s\ell}^d$, as seen in Fig. 9 and 10.

To avoid such bound, we can consider the sizable couplings g_{uu}^L and g_{dd}^L which are almost equal to $|g_{cc}^L| > \mathcal{O}(10^{-1})$. However, the existence of such large diagonal couplings is constrained by the π production processes from the B_s meson. Therefore, the model construction providing the (almost) axial vector-like interaction $Z'c\bar{c}$ is not plausible.

Consequently, the g_{cc} scenario where the Z' coupling to the c -quark pair enhances the $a_{s\ell}^s$ requires the existence of the coupling $|g_{cc}^{L,R}g_{sb}^{L,R}|$ larger than $\mathcal{O}(10^{-3})$ to explain the dimuon charge asymmetry. This parameter space has smaller fine tuning from the ΔM_s compared to the $g_{\tau\tau}$ scenario, due to the interference with the SM process in the contribution to Γ_{12}^s . However, the recent LHCb 1fb^{-1} constraint on $\phi_s^{J/\psi\phi}$ and $\Delta\Gamma_s$, as well as the constraint from $B \rightarrow J/\psi K_S$, is quite strong to demand the (almost) axial vector-like interaction of $Z'c\bar{c}$. On the other hand, the existence of such interaction makes the model construction very hard due to the experimental bounds such as K or D meson mixing and the π production from the B_s decays.

VI. CONCLUSIONS

The like-sign dimuon charge asymmetry has been observed at the D0 which is deviated more than 3σ from the SM prediction. In the recent result in 2011, it was possible to separately detect the flavor specific asymmetry from the B_s and B_d mixing by imposing the impact parameter cut reducing the background. In this paper, we showed that the enhancement of flavor specific asymmetry $a_{s\ell}^s$ is highly constrained by the recent LHCb result with 1fb^{-1} integrated luminosity. We presented the constraints on the Z' couplings $g_{bs}, g_{\tau\tau}$ and/or g_{cc} and the possible enhancement of $a_{s\ell}^s$. The actual upper bound of the couplings are expressed when $M_{Z'} \approx M_Z$. By simple scaling of the ratio $M_{Z'}/M_Z$, our result can be applied to the other mass of Z' as well.

For the flavor specific asymmetry $a_{s\ell}^s$, there are three kinds of criteria. By allowing sizable new physics contribution in B_d system ($a_{s\ell}^d$ is 21 times larger than the SM prediction from NP), $|a_{s\ell}^s/a_{s\ell}^{\text{SM}}| \geq 68$ is needed to be within 1σ region. If there is no new physics in B_d system and the deviation of $A_{s\ell}^b$ is the consequence of B_s system alone, we need $|a_{s\ell}^s/a_{s\ell}^{\text{SM}}| \geq 580$ to be within 1σ region. The central value requires $|a_{s\ell}^s/a_{s\ell}^{\text{SM}}| \geq 950$.

The B_s system is highly constrained by the recent LHCb data. In the absence of the modification in the decay, Γ_{12}^s , the recent LHCb measurement of $\phi_s^{J/\psi\phi}$ strongly constrains the phase of the mixing, M_{12}^s . As a result, the maximum enhancement of $a_{s\ell}^s$ from M_{12}^s alone is at most 40 times the SM prediction which is not enough to be within 1σ even if we allow arbitrary NP contribution to $a_{s\ell}^d$.

The $b \rightarrow c\bar{c}s$ coupling can provide an extra contribution in $\phi_s^{J/\psi\phi}$ from the decay. If the coupling is small enough, the main effect would be to modify the relation between the phase of M_{12}^s and $\phi_s^{J/\psi\phi}$ and the constraint on $\phi_s^{J/\psi\phi}$ can be slightly relaxed. In this case the main impact of $b \rightarrow c\bar{c}s$ is to avoid the constraints on the phase of M_{12}^s from the LHCb measurement of $\phi_s^{J/\psi\phi}$. By allowing the $b \rightarrow c\bar{c}s$ coupling, $a_{s\ell}^s$ can be as large as 50 times the SM prediction, which is still smaller than 68 for the 1σ explanation of the asymmetry with arbitrary $a_{s\ell}^d$.

The Γ_{12}^s is constrained by $\Delta\Gamma^s$ measurement which is basically $\text{Re}(\Gamma_{12}^s)$ when M_{12}^s is almost real. The enhancement of $a_{s\ell}^s$ is mainly from $\text{Im}(\Gamma_{12}^s)$ which can affect the other observables like $B^+ \rightarrow K^+\tau\tau$ in the $g_{\tau\tau}$ scenario and $B_s \rightarrow J/\psi\phi$ in the g_{cc} scenario.

The $g_{\tau\tau}$ scenario where the Z' coupling to the τ pair enhances the $a_{s\ell}^s$ requires the

existence of the coupling $|g_{sb}^{L,R} g_{\tau\tau}^{L,R}|$ larger than about 10^{-2} to explain the dimuon charge asymmetry. Therefore, this parameter space cannot avoid the fine tuning from the ΔM_s constraint $|g_{sb}| \leq 10^{-3}$. In addition, due to the constraint from the $b \rightarrow s\nu\bar{\nu}$ experiments, $|g_{\tau\tau}^L|$ must be as small as 3×10^{-4} . The allowed parameter space explaining the observed $a_{s\ell}^s$ within 1σ (68 times larger than the SM prediction) is marginally consistent with the experimental bounds of $\Delta\Gamma_s$ at the LHCb 1fb^{-1} .

The g_{cc} scenario where the Z' coupling to the c -quark pair enhances the $a_{s\ell}^s$ requires the existence of the coupling $|g_{cc}^{L,R} g_{sb}^{L,R}|$ larger than about 10^{-3} to explain the dimuon charge asymmetry. This parameter space has smaller fine tuning from the ΔM_s compared to the $g_{\tau\tau}$ scenario, due to the interference with the SM process in the contribution to Γ_{12}^s . However, the recent LHCb 1fb^{-1} constraint on $\phi_s^{J/\psi\phi}$ and $\Delta\Gamma_s$, as well as the constraint from $B^0 \rightarrow J/\psi K_S$, are quite strong. So the interaction $Z'c\bar{c}$ must be (almost) axial vector-like. On the other hand, the existence of g_{cc}^L from the axial vector constraints makes the model construction not plausible due to the experimental bounds such as K or D meson mixing and the π production from the B_s decays.

Consequently, it is impossible to explain the 1σ range of like-sign dimuon charge asymmetry using Z' contribution in B_s system without the enhancement in $a_{s\ell}^d$. Even with arbitrary $a_{s\ell}^d$, the g_{cc} scenario demands unrealistic model construction. Therefore, we need to consider the sizable NP contribution in $a_{s\ell}^d$, while making the $a_{s\ell}^s$ as small as possible. To explain the asymmetry within 1σ by minimizing the NP contribution to B_s system, we need the $a_{s\ell}^d$ which is only about 21 times the SM prediction at most, as shown in Fig. 1. So the required off-diagonal coupling $|g_{db}|$ to enhance the $a_{s\ell}^d$ is smaller than the $|g_{sb}|$. On the other hand, the CKM suppression strengthens the experimental bounds except $\Delta\Gamma_d$ which has been poorly measured so far. The experimental bounds to be analyzed contain $B^0 \rightarrow \tau^+\tau^-$, $B \rightarrow \pi\tau^+\tau^-$, and $B_s^0 \rightarrow \bar{K}_0\tau^+\tau^-$ when we consider enhancement in Γ_{12}^d through nonzero $g_{\tau\tau}$ coupling. For the case with nonzero g_{cc} coupling, we need to consider $B \rightarrow J/\psi\pi$ and $B_s \rightarrow \bar{K}_0 J/\psi$, etc. Therefore, more careful analysis is required in the future to investigate this approach.

ACKNOWLEDGMENTS

We thank Radovan Dermíšek for the participation of the project from the beginning to

the final stage. This work was supported by the NRF of Korea No. 2011-0017051 (HK, SS) and No. 2011-0012630 (SS). SS is also supported by TJ Park POSCO Postdoc fellowship.

Appendix A: Calculation of the contribution in to $b \rightarrow s\gamma$

Considering the non-zero value of $g_{bb}^{L,R}$ or $g_{ss}^{L,R}$, we can obtain the upper limit of $|g_{sb}^{L,R}|$ from the $b \rightarrow s\gamma$ penguin constraint, shown in Fig. 11.

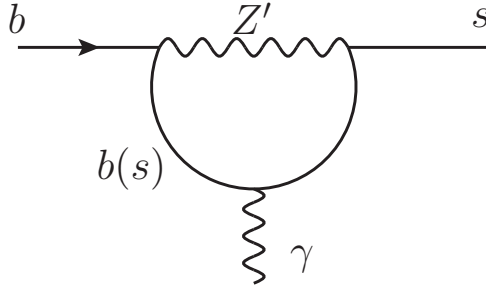


FIG. 11. $b \rightarrow s\gamma$ penguin contribution

The inclusive decay $\Gamma(B \rightarrow X_s\gamma)$ is given approximately by $\Gamma(b \rightarrow X_s^{parton}\gamma)$. The nonperturbative correction to this approximation is smaller than the NNLO perturbative QCD corrections to $\Gamma(b \rightarrow X_s^{parton}\gamma)$. The theoretical prediction for the partonic $\Gamma(b \rightarrow X_s^{parton}\gamma)$ is usually normalized by the semileptonic decay rate to get rid of the uncertainties related to the CKM matrix elements and the fifth power of the b -quark mass. Therefore, the SM NNLO result for a photon-energy cut of $E_\gamma > 1.6 \text{ GeV}$ is obtained as [33]

$$\text{Br}(B \rightarrow X_s\gamma)_{\text{SM}} = (3.15 \pm 0.23) \times 10^{-4} , \quad (\text{A1})$$

while the experimental result with for the same energy cut is measured as [34]

$$\text{Br}(B \rightarrow X_s\gamma)_{\text{exp}} = (3.55 \pm 0.24 \pm 0.09) \times 10^{-4} . \quad (\text{A2})$$

The NP contribution in the total branching ratio is below 30% seeing the result of (A1) and (A2). Therefore, a naive strongest constraint of $|g_{bb}^{L,R}g_{sb}^{L,R}|$ is $< 10^{-2}$ as shown in Fig. 12. However, larger values of the couplings can still satisfy the $b \rightarrow s\gamma$ constraint once the coupling ratio g_{bb}^R/g_{bb}^L is about 1.1 or 1.27. The SM NNLO contribution shows a negligible

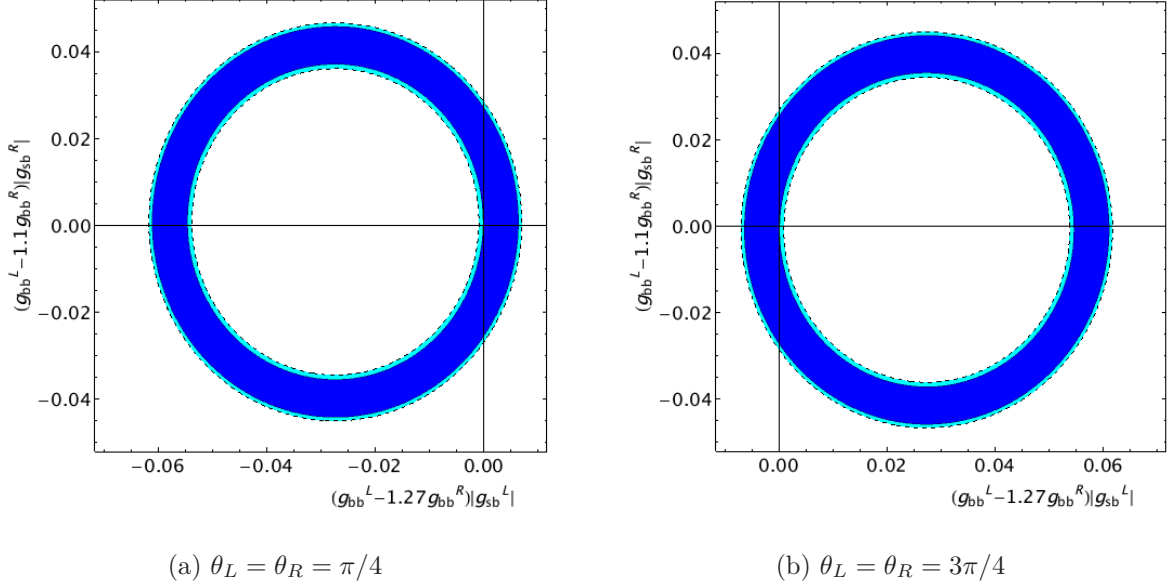


FIG. 12. The limit of the couplings from the experimental bounds of 90% C.L. (Blue) and 95% C.L. (Cyan, Dashed boundary line) of $B \rightarrow X_s \gamma$ for fine-tuned cases (a) $\theta_L = \theta_R = \pi/4$ and (b) $\theta_L = \theta_R = 3\pi/4$.

dependence on the value of μ_b . When the LO NP contribution enhances the SM value by 20%, the μ_b dependence in the total branching ratio induces about 3% uncertainty for $\mu_b = 2.5 - 5$ GeV in the numerical analysis in [35].

Following Eq. (5.3) of [35], the branching ratio with the NP contribution is obtained

$$\begin{aligned} \text{Br}(B \rightarrow X_s \gamma) &= (2.47 \times 10^{-3}) \\ &\times (|C_{7\gamma}(\mu_b)|^2 + |C'_{7\gamma}(\mu_b)|^2 + N(E_\gamma)) , \end{aligned} \quad (\text{A3})$$

where $N(E_\gamma) = (3.6 \pm 0.6) \times 10^{-3}$ is a nonperturbative contribution. Considering the LO NP contributions

$$C_{7\gamma}(\mu_b) = C_{7\gamma}^{\text{SM}}(\mu_b) + \Delta C_{7\gamma}(\mu_b) , \quad (\text{A4})$$

where the central value of the SM contribution is calculated at the NNLO level for $\mu_b = 2.5$ GeV such that

$$C_{7\gamma}^{\text{SM}}(\mu_b) = -0.3525 . \quad (\text{A5})$$

The NP contribution is obtained as following.

$$\begin{aligned} \Delta C_{7\gamma}(\mu_b) = \frac{1}{g_1^2} \frac{M_Z^2}{M_{Z'}^2} \frac{1}{V_{tb} V_{ts}^*} \times \left[\left(-\frac{2}{9} \kappa_7 + \frac{2}{3} \kappa_8 \right) g_{ss}^L g_{sb}^L - 2\kappa_{LL}^s g_{ss}^L (g_{sb}^L)^* \right. \\ \left. + \left(-\frac{2}{9} \kappa_7 + \frac{2}{3} \kappa_8 - 2\kappa_{LL}^b \right) g_{bb}^L (g_{sb}^L)^* + \left(\frac{2}{3} \kappa_7 - 2\kappa_8 - 2\kappa_{LR}^b \right) g_{bb}^R (g_{sb}^L)^* \right. \\ \left. + \left(\frac{2}{3} \kappa_7 - 2\kappa_8 \right) \frac{m_s}{m_b} g_{ss}^L g_{sb}^R - 2\kappa_{LR}^s g_{ss}^R (g_{sb}^L)^* \right] , \end{aligned} \quad (\text{A6})$$

where κ 's are listed in Table 1 of [35]. The prime coefficients are obtained as

$$C_{7\gamma}^{\text{SM}}(\mu_b) = -0.3523 \frac{m_s}{m_b} , \quad (\text{A7})$$

$$\begin{aligned} \Delta C_{7\gamma}'(\mu_b) = \frac{1}{g_1^2} \frac{M_Z^2}{M_{Z'}^2} \frac{1}{V_{tb} V_{ts}^*} \left[\frac{2m_s}{9m_b} (-\kappa_7 + 3\kappa_8) g_{ss}^R g_{sb}^R - 2\kappa_{LL}^s g_{ss}^R (g_{sb}^R)^* \right. \\ \left. + \left(\frac{2m_s}{9m_b} (-\kappa_7 + 3\kappa_8) - 2\kappa_{LL}^b \right) g_{bb}^R (g_{sb}^R)^* \right. \\ \left. + \left(\frac{2}{3} \frac{m_s}{m_b} \kappa_7 - 2 \frac{m_s}{m_b} \kappa_8 - 2\kappa_{LR}^b \right) g_{bb}^L (g_{sb}^R)^* + \left(\frac{2}{3} \kappa_7 - 2\kappa_8 \right) \left(\frac{m_s}{m_b} \right)^2 g_{ss}^R g_{sb}^L - 2\kappa_{LR}^s g_{ss}^L (g_{sb}^R)^* \right] . \end{aligned} \quad (\text{A8})$$

In the simple case that $g_{ss}^{L,R} = 0$ and our values of κ s are not much different from those with the matching scale at around 200 GeV. We obtain the following result,

$$C_{7\gamma} = -0.3523 - 9.11 \times (g_{bb}^L - 1.27g_{bb}^R)(g_{sb}^L)^* , \quad (\text{A9})$$

$$C_{7\gamma}' = -0.3523 \frac{m_s}{m_b} + 6.83 \times (g_{bb}^L - 1.1g_{bb}^R)(g_{sb}^R)^* . \quad (\text{A10})$$

Plugging (A9) into (A3) with the consideration of the experimental limit (A2), we can obtain the limit of $(g_{bb}^L - 1.27g_{bb}^R)|g_{sb}^L|$ and $(g_{bb}^L - 1.1g_{bb}^R)|g_{sb}^R|$ according to a fixed value of the (θ_L, θ_R) such that

$$\begin{aligned} 6.42(g_{bb}^L - 1.27g_{bb}^R)|g_{sb}^L| \cos \theta_L + 82.99(g_{bb}^L - 1.27g_{bb}^R)^2 |g_{sb}^L|^2 \\ - 0.11(g_{bb}^L - 1.1g_{bb}^R)|g_{sb}^R| \cos \theta_R + 46.65(g_{bb}^L - 1.1g_{bb}^R)^2 |g_{sb}^R|^2 = 0.016 \pm 0.01 , \end{aligned} \quad (\text{A11})$$

within 1σ up to $\mathcal{O}(10^{-4})$, calculated with $m_s = 100$ MeV and $m_b = 4.2$ GeV.

Appendix B: The effect of the theoretical uncertainties in the form factors

Considering the square root error propagation, this uncertainty changes the quantity k_{\pm} to 1/3 or twice of the original calculation. (For the Ball-Zwicky model, $k_+ = (8.02A_1 + 3.35Z)/(8.02A_1 - 3.35Z)$ for the form factors A_1, Z in [16]. Considering the 10 % uncertainties, $k_+ = (8.02 \cdot 0.42(1 \pm 0.1) + 3.35 \cdot 0.82(1 \pm 0.1))/(8.02 \cdot 0.42(1 \pm 0.1) - 3.35 \cdot 0.82(1 \pm 0.1))$. Simple calculation with $A_1 = 0.42(1 - 0.9)$ and $Z = 0.82(1 + 0.1)$ can make k_+ very large as 518. However, the error propagation without considering the covariance can make it smaller.

$$\begin{aligned}
k_+ &= \frac{8.02 \cdot 0.42 + 3.35 \cdot 0.82 \pm \sqrt{(8.02)^2(0.042)^2 + (3.35)^2(0.082)^2}}{8.02 \cdot 0.42 - 3.35 \cdot 0.82 \pm \sqrt{(8.02)^2(0.042)^2 + (3.35)^2(0.082)^2}} \\
&= \frac{8.02 \cdot 0.42 + 3.35 \cdot 0.82}{8.02 \cdot 0.42 - 3.35 \cdot 0.82} \left(1 \pm \sqrt{\frac{(8.02)^2(0.042)^2 + (3.35)^2(0.082)^2}{(8.02 \cdot 0.42 + 3.35 \cdot 0.82)^2}} \right) \\
&\quad \times \sqrt{\frac{1}{(8.02 \cdot 0.42 + 3.35 \cdot 0.82)^2} + \frac{1}{(8.02 \cdot 0.42 - 3.35 \cdot 0.82)^2}} \\
&= 9.83(1 \pm 0.70) ,
\end{aligned} \tag{B1}$$

which makes $k_+ = 2.9 - 16.7$.) The ratio of each polarized amplitude can be obtained in the CDF data where the transverse amplitude $A_{\parallel, \perp} = (A_+ + A_-)/\sqrt{2}$ [32].

Appendix C: Calculation of the contribution to $b \rightarrow s\nu\bar{\nu}$

All the observables depend on the complex Wilson coefficient C_L and C_R such that

$$\text{Br}(B \rightarrow K^* \nu \bar{\nu}) = 6.8 \times 10^{-6} (1 + 1.31\eta) \epsilon^2 , \tag{C1}$$

$$\text{Br}(B \rightarrow K \nu \bar{\nu}) = 4.5 \times 10^{-6} (1 - 2\eta) \epsilon^2 , \tag{C2}$$

$$\text{Br}(B \rightarrow X_s \nu \bar{\nu}) = 2.7 \times 10^{-5} (1 + 0.09\eta) \epsilon^2 , \tag{C3}$$

where ϵ and η are

$$\epsilon = \frac{\sqrt{|C_L|^2 + |C_R|^2}}{|(C_L)^{\text{SM}}|} , \tag{C4}$$

$$\eta = \frac{-\text{Re}(C_L C_R^*)}{|C_L|^2 + |C_R|^2} . \tag{C5}$$

The Wilson coefficients are

$$C_L = (C_L)^{\text{SM}} + (C_L)^{\text{NP}} \equiv (C_L)^{\text{SM}} - \frac{1}{2} \frac{1}{\frac{\alpha}{2\pi} V_{tb} V_{ts}^*} \frac{1}{g_1^2} \frac{M_Z^2}{M_{Z'}^2} g_{\nu\nu} g_{sb}^L , \tag{C6}$$

$$C_R = -\frac{1}{2} \frac{1}{\frac{\alpha}{2\pi} V_{tb} V_{ts}^*} \frac{1}{g_1^2} \frac{M_Z^2}{M_{Z'}^2} g_{\nu\nu} g_{sb}^R , \tag{C7}$$

where $(C_L)^{\text{SM}} = -6.83 \pm 0.06$. It is clearly seen that the SM prediction is obtained when $\eta = 0$ and $\epsilon = 1$.

-
- [1] V. M. Abazov *et al.* [D0 Collaboration], Phys. Rev. **D82**, 032001 (2010) [arXiv:1005.2757 [hep-ex]].
 - [2] V. M. Abazov *et al.* [D0 Collaboration], Phys. Rev. D **84**, 052007 (2011) [arXiv:1106.6308 [hep-ex]].
 - [3] A. Lenz and U. Nierste, [arXiv:1102.4274 [hep-ph]].
 - [4] J. E. Kim, M. -S. Seo and S. Shin, Phys. Rev. **D83**, 036003 (2011) [arXiv:1010.5123 [hep-ph]].
 - [5] A. K. Alok, S. Baek and D. London, JHEP **1107**, 111 (2011) [arXiv:1010.1333 [hep-ph]].
 - [6] C. W. Bauer and N. D. Dunn, Phys. Lett. **B696**, 362-366 (2011) [arXiv:1006.1629 [hep-ph]].
 - [7] J. E. Kim and S. Shin, Phys. Rev. D **85**, 015012 (2012) [arXiv:1104.5500 [hep-ph]].
 - [8] X. -Q. Li, Y. -M. Li, G. -R. Lu and F. Su, arXiv:1204.5250 [hep-ph].
 - [9] A. Lenz and U. Nierste, JHEP **0706**, 072 (2007) [hep-ph/0612167].
 - [10] E. Barberio *et al.* [Heavy Flavor Averaging Group Collaboration], [arXiv:0808.1297 [hep-ex]].
 - [11] R. Dermisek, S. -G. Kim and A. Raval, Phys. Rev. D **84**, 035006 (2011) [arXiv:1105.0773 [hep-ph]] ; R. Dermisek, S. -G. Kim and A. Raval, Phys. Rev. D **85**, 075022 (2012) [arXiv:1201.0315 [hep-ph]].
 - [12] X. -G. He and G. Valencia, Phys. Rev. D **74**, 013011 (2006) [hep-ph/0605202].
 - [13] V. Barger, C. W. Chiang, J. Jiang and P. Langacker, Phys. Lett. B **596**, 229 (2004) [arXiv:hep-ph/0405108].
 - [14] K. Nakamura *et al.* (Particle Data Group), Journal of Physics G37, 075021 (2010) and 2011 partial update for the 2012 edition.
 - [15] LHCb-CONF-2012-002
 - [16] C. -W. Chiang, A. Datta, M. Duraisamy, D. London, M. Nagashima and A. Szykman, JHEP **1004**, 031 (2010) [arXiv:0910.2929 [hep-ph]].
 - [17] S. Burdin [D0 Collaboration], “Measurements of CP violation in the B_s system at D0”, talk given at the Europhysics Conference on High-Energy Physics 2011, July 21, 2011.
 - [18] D. Melikhov and B. Stech, Phys. Rev. D **62**, 014006 (2000) [hep-ph/0001113].
 - [19] P. Ball and R. Zwicky, Phys. Rev. D **71**, 014029 (2005) [hep-ph/0412079].

- [20] C. Bobeth and U. Haisch, [arXiv:1109.1826 [hep-ph]].
- [21] W. Altmannshofer, A. J. Buras, D. M. Straub, M. Wick, JHEP **0904**, 022 (2009) [arXiv:0902.0160 [hep-ph]].
- [22] W. Altmannshofer, P. Paradisi and D. M. Straub, JHEP **1204**, 008 (2012) [arXiv:1111.1257 [hep-ph]].
- [23] R. Barate *et al.* [ALEPH Collaboration], Eur. Phys. J. C **19**, 213 (2001) [hep-ex/0010022].
- [24] P. J. Fox, J. Liu, D. Tucker-Smith and N. Weiner, Phys. Rev. D **84**, 115006 (2011) [arXiv:1104.4127 [hep-ph]].
- [25] J. Charles *et al.* [CKMfitter Group Collaboration], Eur. Phys. J. **C41**, 1-131 (2005) [hep-ph/0406184].
- [26] E. Lunghi and A. Soni, arXiv:1104.2117 [hep-ph]; E. Lunghi and A. Soni, Phys. Lett. B **697**, 323 (2011) [arXiv:1010.6069 [hep-ph]].
- [27] E. Golowich, S. Pakvasa and A. A. Petrov, Phys. Rev. Lett. **98**, 181801 (2007) [hep-ph/0610039].
- [28] S. -L. Chen, X. -G. He, A. Hovhannisyan *et al.*, JHEP **0709**, 044 (2007) [arXiv:0706.1100 [hep-ph]].
- [29] A. Zupanc, K. Abe, K. Abe, H. Aihara, D. Anipko, K. Arinstein, V. Aulchenko and T. Aushev *et al.*, Phys. Rev. D **75**, 091102 (2007) [hep-ex/0703040].
- [30] G. F. Giudice, G. Isidori and P. Paradisi, JHEP **1204**, 060 (2012) [arXiv:1201.6204 [hep-ph]].
- [31] W. Altmannshofer, R. Primulando, C. -T. Yu and F. Yu, JHEP **1204**, 049 (2012) [arXiv:1202.2866 [hep-ph]].
- [32] D. Acosta *et al.* [CDF Collaboration], Phys. Rev. Lett. **94**, 101803 (2005) [arXiv:hep-ex/0412057].
- [33] M. Misiak, H. M. Asatrian, K. Bieri, M. Czakon, A. Czarnecki, T. Ewerth, A. Ferroglia and P. Gambino *et al.*, Phys. Rev. Lett. **98**, 022002 (2007) [hep-ph/0609232].
- [34] D. Asner *et al.* [Heavy Flavor Averaging Group Collaboration], arXiv:1010.1589 [hep-ex].
- [35] A. J. Buras, L. Merlo and E. Stamou, JHEP **1108** (2011) 124 [arXiv:1105.5146 [hep-ph]].